

Research Article

Utilizing Local Waste: Sustainable Adsorption of Reactive Blue 235 on Surfactant-Modified Bamboo Fibers

Samriti Vaid ¹, Varinder Kaur ², Sanyog Sharma ¹, Anupinder Singh ³,
Bhavna Vaid ⁴, Raj Kumar Arya ⁵, and G. D. Verros ⁶

¹Department of Chemistry, UGC Sponsored-Centre for Advanced Studies-II, Guru Nanak Dev University, Amritsar 143005, Punjab, India

²Department of Apparel and Textile Technology, Guru Nanak Dev University, Amritsar 143005, Punjab, India

³Department of Physics, Guru Nanak Dev University, Amritsar 143005, Punjab, India

⁴PG Department of Chemistry, Sri Guru Teg Bahadur Khalsa College, Anandpur Sahib 140118, Punjab 160062, India

⁵Department of Chemical Engineering, Dr. B.R. Ambedkar National Institute of Technology, Jalandhar 144011, Punjab, India

⁶Laboratory of Polymer and Colour Chemistry and Technology, Department of Chemistry, Aristotle University of Thessaloniki, P.O. Box 454, Plagiari 57500, Greece

Correspondence should be addressed to Varinder Kaur; varinder_gndu@yahoo.com and Raj Kumar Arya; aryark@nitj.ac.in

Received 9 January 2024; Revised 21 February 2024; Accepted 18 March 2024; Published 18 April 2024

Academic Editor: Abdussalam Elhanashi

Copyright © 2024 Samriti Vaid et al. This is an open access article distributed under the Creative Commons Attribution License, which permits unrestricted use, distribution, and reproduction in any medium, provided the original work is properly cited.

In this research endeavor, we sought to enhance the efficacy of bamboo fibers through modification with the surfactant cetyltrimethylammonium bromide (CTAB) for the purpose of removing Reactive Blue 235 from effluent. Our investigation encompassed a comprehensive exploration of the impact of crucial parameters, namely, adsorbent dosage (0.25 g–1.25 g), contact time (10–80 min), pH (2–12), initial dye concentration (20–100 mg/L), and temperature (298 K, 308 K, and 318 K) on the dynamics of dye removal. The optimum dye removal efficiency of 94% for Reactive Blue 235 was obtained at an adsorbent dosage of 0.5 g/50 ml of dye solution, initial dye concentration of 40 mg/L, pH of 6, and contact time of 40 min. The experimental framework included the anticipation of data aligned with various isothermal and kinetic models, facilitating a nuanced understanding of the adsorption process. Our findings unveiled that the kinetics of adsorption adhered to a second-order model, while the Langmuir isotherm model aptly described the adsorption behavior. Particularly noteworthy was the monolayer's adsorption capacity, quantified at an impressive $7.39 \text{ mg}\cdot\text{g}^{-1}$ at a temperature of 318 K. The value of Freundlich's constant, K_F , increases with an increase in temperature indicating the endothermic nature of adsorption. The magnitude of E obtained from Dubinin–Radushkevich isotherm varying from 3.92 to 4.66 kJ/mol on increasing temperature from 298 K to 318 K suggests that adsorption of RB235 on BAT is a physisorption (value of E is between 1 and 8 kJ/mol). Delving into the thermodynamic aspects of the process, we calculated ΔH and ΔS to be 54.88 kJ/mol and 184.54 J/mol/K, respectively. The consistently negative values of ΔG (between -0.183 kJ/mol and -3.884 kJ/mol) at all temperatures underscored the feasibility, spontaneity, and entropy-driven nature of the adsorption of RB235 on CTAB-treated bamboo fiber (BAT). What sets our study apart is the deliberate utilization of bamboo fibers sourced from local waste streams, embodying a commitment to sustainable practices. Beyond its effectiveness in effluent treatment, our approach aligns with eco-friendly principles by repurposing indigenous waste materials, contributing to a more sustainable and environmentally responsible future.

1. Introduction

The discharge of effluents from textile industries poses substantial risks to both human and aquatic life [1–4]. Annually, the global fabric industry manufactures

approximately 7×10^7 tons of artificial dyes, with approximately 10% released as environmental effluent after dyeing and processing [5, 6]. Dyes find extensive applications in the printing, cosmetics, textile, pharmaceutical, leather, and food sectors. The hazardous and nonbiodegradable nature of

various organic dyes raises concerns for both the aquatic environment and human health [7]. Notably, 40–50% of applied dyes persist in the liquid phase, contributing to environmental pollution [2].

Dyes can be classified as anionic (direct, acid, and reactive dyes), cationic (basic dyes), and nonionic (disperse dyes) [5]. However, reactive azo dyes constitute over 50% of all textile dyes used in the industry, and they are characterized by the existence of nitrogen-nitrogen double bonds (-N=N-) [6, 7]. Among all the textile dyes, reactive dyes impose difficulty in removing from the effluent as these dyes are excessively water soluble [8]. Several industries are encouraged to use these dyes because of their unique properties, which include vibrant colors, outstanding colorfastness, and ease of use [9]. Despite the reality that reactive dyes are highly toxic and can cause allergic reactions in the eyes, skin, mucous membranes, and upper respiratory tract [9], as well as the fact that a small amount of dye is hydrolyzed during dyeing (15–40%), they are still widely used in the textile industry since they are highly stable and have a very good ability to bind via formation of covalent bond with the textile fibers considering they contain many reactive groups in their chemical structure [10].

Thus, an array of technologies, including coagulation/flocculation [11, 12], filtration [13], adsorption [14], constructed wetlands [15, 16], advanced oxidation process (AOP) [17], sonophotocatalytic degradation [18], activated sludge process (ASP) [19, 20], sequencing batch reactors (SBRs) [20, 21], membrane bioreactors (MBRs) [22], and ion-exchange [23, 24], are reported to be used for the removal of dyes from wastewater.

Among these technologies, adsorption stands out as one of the most efficient and straightforward techniques for removing dyes from effluents. Its advantages include simplicity, environmental friendliness, low cost, and, in most cases, the reusability of the adsorbent [25]. During adsorption, dye molecules in the liquid phase move into the solid phases of various adsorbents [26]. The effectiveness of adsorption technology hinges on the development of efficient adsorbents.

Diverse materials have been explored as adsorbents to remove dye effluents, including activated carbon [27–29], hybrid nanomaterials [30, 31], bio-adsorbents [32–35], metal-organic frameworks [36], carbon nanotubes [37], and polymers and their nanocomposites [38, 39], among others.

Various adsorbents, including surfactant-modified ones, have been employed to address the removal of reactive dyes [40–60].

Over the years, researchers have explored the use of agricultural wastes, such as rice husk, wheat straw, rice peel, sugar cane bagasse, orange peel, and garlic peel, for dye removal [61–64]. Naturally occurring fiber-based materials, including cotton fibers, kapok, kenaf core, and palm kernel, have also been investigated as adsorbents for dye removal [65–68].

Bamboo, classified as a lignocellulosic biomass fiber [69, 70], shares characteristics with other bast fibers like jute and flax concerning chemical composition and physical qualities. Comprising extractives such as protein, pectin, and

wax (2–3%), along with cellulose (70–74%), hemicellulose (12–14%), and lignin (10–12%), bamboo fibers exhibit unique properties. Notably, bamboo fibers boast a higher water-holding capacity than traditional fibers like cotton and flax, making bamboo a promising material for adsorption applications.

Previous literature has explored the adsorption capabilities of carbon fiber aerogel derived from natural bamboo fibers, highlighting the potential of bamboo in capturing oils and organic solvents [70–73]. Studies have also reported successful dye removal using bamboo-based activated carbons [74–77], bamboo-based biochar [78, 79], and carbonized bamboo leaf powder [80].

Building on this groundwork, our current study focuses on harnessing the potential of bamboo waste obtained from Unati Bamboo Mission (Mission to develop, train, and deliver Bamboo Products). Specifically, we employ cetyltrimethylammonium bromide (CTAB) to treat these bamboo fibers. These treated fibers, designated as bamboo after treatment (BAT), serve as an adsorbent for removing Reactive Blue 235 (RB235) color from textile effluent. Significantly, the utilization of bamboo fibers treated with CTAB for reactive dye removal from effluent represents an innovative approach with potential sustainability implications.

The primary objectives of our research underscore the importance of local bamboo waste: (1) evaluate the practicality of BAT as an adsorbent for removing Reactive Blue 235 dye; (2) characterize the prepared adsorbents through various techniques; (3) investigate parameters influencing the dye removal percentage; and (4) assess the applicability of kinetic and isothermal models for the adsorption data. By emphasizing the local bamboo waste as a key component of our study, we aim to contribute not only to effective dye removal but also to sustainable waste utilization practices within the context of textile industry effluent treatment.

2. Materials and Methods

2.1. Materials. Bamboo fibers were obtained from Bambuka Under Unnati (Mission to develop, train, and deliver Bamboo Products). Cetyltrimethylammonium bromide (CTAB) was the surfactant used and was purchased from Loba Chemie Laboratory Reagents & Fine Chemicals (CAS No. 57-09-0 and purity = 99%), and sodium hydroxide pellets (CAS No. 1310-73-2 and minimum assay of 98%) was obtained from SiscoResearch Laboratories Pvt. Ltd. A Remazol dye Novacron Blue FNR (C.I. name = Reactive Blue 235, PubChem CID: 138394484, Molecular formula = $C_{29}H_{25}CuFN_9Na_3O_{12}S_3^{+2}$, molecular weight = 939.3), which is a copper complex of Formazan Reactive dye with mono-fluoro triazine and vinyl sulfonyl reactive groups (bifunctional dye) were used in our study. The dye was provided by Colour-Chem India Pvt. Ltd. (triazine). During this study, all the other chemicals used were of analytical grade.

2.2. Preparation of Adsorbents. Bamboo fibers obtained from Bambuka Under Unnati were allowed to dry at 60°C for 24 hours in order to completely eliminate any moisture that

might have been retained inside. To boost their absorbency, these fibers underwent additional modifications. In order to achieve this, 20 g of dried bamboo fibers (BBT) was taken and put into a beaker containing 1.14 g of CTAB dissolved in 500 ml of distilled water. After that, the entire mixture was allowed to shake for 24 hours at room temperature (25°C). The suspension was left undisturbed for 10 minutes, and then the liquid was discarded. After that, the surfactant that had been superficially bonded to the treated bamboo fibers was removed by repeatedly washing them in distilled water. Furthermore, these CTAB-treated bamboo fibers (BAT) were dried in a hot air oven for 24 hours at 60°C.

2.3. Preparation of the Dye Solution. Remazol dye Reactive Blue 235 was used without further purification. A stock solution of dye (100 mg/L) was prepared in distilled water. By dilution with distilled water, a number of the necessary concentrations were created consecutively from this stock solution. The electronic absorption spectra were recorded on a Shimadzu UV-1900 UV-vis spectrophotometer.

2.4. Characterization of Adsorbents. The Fourier transform infrared (FT-IR) spectra were noted in the range of 4000 – 400 cm⁻¹ on Agilent technology Cary 630 spectrophotometer using ATR technique. The samples were further characterized by X-ray diffraction using XRD Rigaku miniflex 2 analytical instruments functioned with a current of 30 mA and at 40 kV with Cu-K α radiation ($\lambda = 1.5406 \text{ \AA}$). The specific surface area of the adsorbents was calculated using the BET method (Brunauer–Emmett–Teller) in accordance with the BET equation, assuming that the nitrogen molecule has an area of 0.162 nm². Surface morphology of BBT, BAT, and bamboo fibers after treatment with CTAB loaded with Reactive Blue 235 dye (RB-BAT) was analyzed under a Carl Zeiss FE-SEM (Scanning Electron Microscope). The SEM was operated at 10 kV and 50 microAmp for anode voltage and beam current, respectively. The thermal stability of BBT, BAT, and RB-BAT was evaluated; approximately 2 mg of compounds was analyzed using a thermogravimetric analyzer (model HITACHI STA7200). The heating was done as described from 22 to 800°C at a rate of 10°C/min under 250 ml/min flow rate of nitrogen.

Zero-point charge pH (pH_{zpc}) plays a critical role in the adsorption process. Utilizing the drift method [81], the pH_{zpc} of BBT and BAT was determined. In a 100 ml volumetric flask, 50 ml of a 0.01 M sodium chloride solution was used for this experiment. Successive NaCl solutions of various pH values from 12 to 2 pH were prepared by employing either 0.1 N of sodium hydroxide for alkaline pH and 0.1 N of hydrochloric acid for acidic pH. Adsorbents (0.15 g) were immersed to each 50 ml NaCl solution (from pH 2 to 12). We measured the final pH and plotted it versus the change in pH after a 24-hour contact time. As is reported, the point of zero charge, pH_{zpc} (pH_{Final} = pH_{Initial}), is defined as the pH where the curve crosses the line.

Boehm titration methods were used to ascertain the surface chemistry [82]. 50 ml of 0.01 M sodium bicarbonate was mixed with 100 mg of BAT. Similarly, 50 ml of hydrochloric acid, sodium hydroxide, and sodium carbonate of 0.01 M each were mixed with 100 mg of BAT. These mixtures were kept for agitation at 298 K and 100 rpm for 24 hours separately. For calculating the acidic groups present in BAT, the aliquots were back-titrated with 0.01 M hydrochloric acid, whereas for determining basic groups, titration was done using 0.01 M NaOH. The neutralization points were determined by applying phenolphthalein as an indicator for strong base and strong acid titration and methyl red for strong acid and weak base titration. It is assumed that only carboxylic acid groups are neutralized by sodium bicarbonate, and both carboxylic and lactonic groups are neutralized by sodium carbonate, whereas carboxylic, lactonic, and phenolic groups are neutralized by sodium hydroxide [82].

2.5. Batch Adsorption Study. Adsorption studies were done in batches to determine the impact of various factors such as adsorbent dosage, contact time, pH, initial concentration of dye, and temperature on the adsorption of Reactive Blue 235 onto adsorbents BBT and BAT. The experimental circumstances studied were pH (2–12), contact time (10 min–80 min), adsorbent dosage (0.25 g–1.25 g), dye concentration (20 mg/L to 100 mg/L), and temperature (298 K, 308 K, and 318 K). A conical flask was filled with 50 ml of a known concentration dye solution, and the required quantities of adsorbent were added and shaken at predefined conditions. Following that, the liquid supernatant was filtered, and the quantity of dye extracted from the dye solution and subsequently adsorbed on BBT and BAT was calculated spectrophotometrically ($\lambda_{\text{max}} = 612 \text{ nm}$). A most favorable set of experimental factors such as adsorbent dosage (0.5 g), contact time (60 minutes), pH (7.0), stirring speed (180 rpm), dye concentration (40 mg/L), and temperature (298 K) was used in all experiments except wherever mentioned differently.

Batch equilibrium and kinetic studies were done by shaking a 50 ml dye solution of various dye concentrations at pH 7.0 with 0.5 g of adsorbents at 298 K, 308 K, and 318 K, respectively. The adsorption capacity at equilibrium (q_e), at any time (q_t), and % dye removal were determined using the following equations:

$$\text{Adsorption capacity at equilibrium, } q_e = (C_o - C_e) X \frac{V}{w},$$

$$\text{Adsorption capacity at any time, } q_t = (C_o - C_t) X \frac{V}{w}, \quad (1)$$

$$\% \text{ dye removal} = (C_o - C_e) X \frac{100}{C_o},$$

where C_o is the initial concentration of the dye, C_e is concentration of the dye at equilibrium, C_t is the concentration of dye at any time, V is the dye solution's volume taken in litres, and w is the mass of BBT or BAT.

3. Results and Discussion

3.1. Characterization of Bamboo Fibers (Treated BAT and Untreated BBT)

3.1.1. pH_{ZPC} and Surface Functional Groups. The determination of the point of zero charge (pH_{ZPC}) for BBT and BAT was conducted through the drift method. The calculated pH_{ZPC} value for BBT and BAT was found to be 5.2 and 8.5, respectively (refer to Figure 1). This value signifies that at pH levels below the pH_{ZPC} , the BBT and BAT surface carries a positive charge, while at pH levels above the pH_{ZPC} , the surface exhibits a negative charge. This observation is critical for understanding the optimal conditions for adsorption.

Figure 1 illustrates the pH_{ZPC} of BBT and BAT, highlighting the transition from a negatively charged surface to a positively charged one. Notably, the pH_{ZPC} of BBT is less than 7 which signifies that the surface of BBT is negatively charged, whereas the pH_{ZPC} of BAT is more than 7 suggesting the positively charged surface of BAT as depicted in Figure 1(c) [83]. Given the anionic nature of the dye used in this study, effective adsorption is favored when the surface of the adsorbent is positively charged. Conversely, when the surface becomes negatively charged, repulsion between anionic dye molecules and the adsorbent surface hinders the adsorption process [84]. Thus, the treatment of BBT with surfactant CTAB helps in converting the charge on the surface of bamboo fibers from negative to positive, thus enhancing the affinity of anionic dye molecules towards the adsorbent [85].

In an aqueous medium, BBT was found to have a pH of 5.7 suggesting its somewhat acidic nature [86], whereas BAT was observed to have a pH of 7.9, suggesting its basic nature. This is further supported by both the pH and pH_{ZPC} values. The Boehm titration results for BAT revealed a higher quantity of basic groups compared to acidic groups, confirming the overall basic nature of BAT. Specifically, the total functionalized groups, acidic groups, and basic groups were determined to be 3.18 mmol/g, 0.48 mmol/g, and 2.7 mmol/g, respectively. This comprehensive characterization of pH_{ZPC} and surface functional groups provides valuable insights into the electrochemical properties of BBT and BAT, laying the groundwork for understanding its adsorption behavior in subsequent analysis.

3.1.2. FT-IR Studies. Fourier transform infrared (FT-IR) analysis stands as a pivotal technique for elucidating information regarding the functional groups and various bonds within materials [87, 88]. Figure 2 presents the FT-IR spectra of bamboo before treatment (BBT), bamboo after treatment (BAT), and Reactive Blue-loaded BAT (RB-BAT). The spectral features offer crucial insights into the chemical composition and structural changes induced by the treatment processes.

The absorption band observed around 3324 cm^{-1} (in case of RB-BAT) is attributed to O-H stretching vibration. This stretching vibration is likely associated with hydroxyl groups present in cellulose, hemicellulose, lignin, extractives, and carboxylic acids. It can be seen from Figure 2 that

the band of O-H stretching vibration has shifted from 3338 cm^{-1} in case of BBT to 3333 cm^{-1} in case of BAT and finally to 3324 cm^{-1} in RB-BAT. The band at approximately 2905 cm^{-1} corresponds to C-H stretching, a characteristic feature of natural fibers.

Furthermore, distinct bands at 1739 cm^{-1} (present in BBT and BAT but absent in RB235) and around 1632 cm^{-1} (RB-BAT) are indicative of C=O stretching. These bands in the spectra are likely attributed to the vibration of the α -keto carbonyl for cellulose. As seen in Figure 2, the band at 1665 cm^{-1} (in BBT) shifted to 1661 cm^{-1} (in BAT) and finally diminished a lot in case of RB-BAT. The band at 1638 cm^{-1} in BBT gets shifted to 1632 cm^{-1} in case of RB-BAT and also this band has become more prominent in case of RB-BAT. The presence of an absorption band at 1421 cm^{-1} (in RB-BAT) which was at 1429 cm^{-1} (in BBT) suggests an aromatic ring vibration. The band at 1365 cm^{-1} (in BBT) shifted to 1362 cm^{-1} in case of RB-BAT. The band at 1323 cm^{-1} may be associated with C-H deformation in lignin. Additionally, the band at 1161 cm^{-1} (in BAT) has shifted to 1153 cm^{-1} (in RB-BAT) which is a potential indication of C-O stretching in conjugated ester groups within lignins. Lastly, the band at 1028 cm^{-1} corresponds to C-H and C-O deformation.

The comparison of FT-IR spectra between BBT, BAT, and RB-BAT provides a comprehensive understanding of the chemical changes occurring during the treatment process and subsequent dye loading. This detailed analysis aids in elucidating the functional groups involved in the adsorption mechanism and provides a foundation for interpreting the adsorption behavior in subsequent sections of the study.

3.1.3. X-Ray Diffraction Study. The X-ray diffraction (XRD) technique serves as a powerful tool for discerning the nature of materials based on their crystallinity or amorphousness. Crystalline materials exhibit well-defined peaks, whereas amorphous or noncrystalline materials manifest broad peaks rather than sharp ones.

Figure 3 illustrates the XRD spectra of bamboo before treatment (BBT), bamboo after treatment (BAT), Reactive Blue-loaded BAT (RB-BAT), and the Reactive Blue 235 (RB235) reference. Notably, both BBT and BAT showcase a slightly crystalline nature. To delve deeper into the crystallite size, the Scherer formula [89] was employed:

$$D = \frac{K\lambda}{\beta \cos \theta} \quad (2)$$

where K is the shape factor, λ is the wavelength of X-ray, β is the line broadening at half the maximum intensity (FWHM) in radians, and θ is the Bragg angle.

Despite the slight crystallinity observed, no significant change in the amorphousness or crystallinity of bamboo fibers was noted after treatment with a surfactant or subsequent dyeing, and T was found to be 3.67 nm, 2.98 nm, and 3.18 nm, respectively. The dimensionless shape is evident in Figure 3. The calculated crystallite size for BBT, BAT, and RB-BAT factor, typically around 0.9, varies with the actual shape of the crystallite. Importantly, the crystallite size is inversely proportional to the peak width.

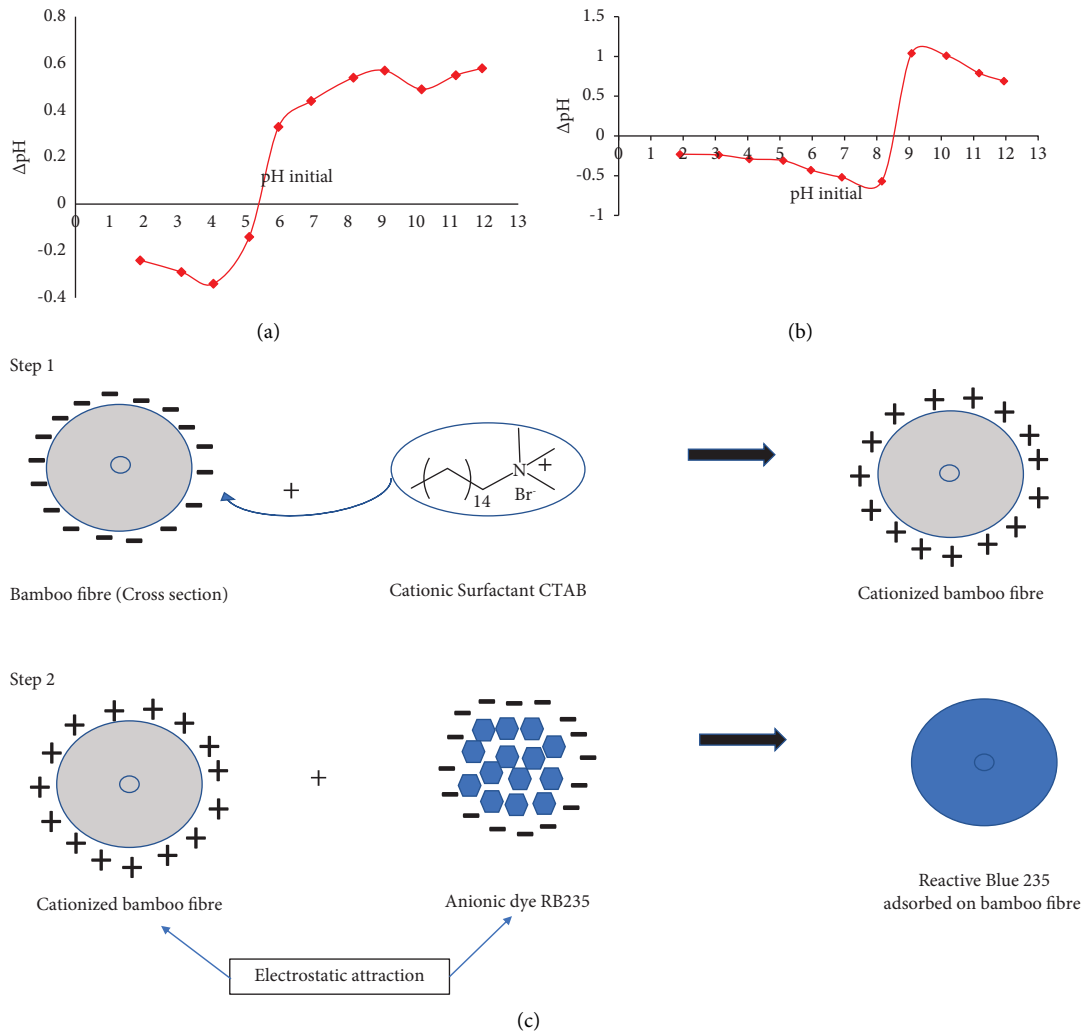


FIGURE 1: Point of zero charge (pH_{ZPC}) of (a) BBT and (b) BAT. (c) Role of surfactant in changing the surface charge of bamboo fibers.

The XRD results affirm the resilience of bamboo fibers' crystallinity, suggesting that their structural integrity remains relatively unchanged after surfactant treatment and dye loading. This information is vital for understanding the stability and structural characteristics of bamboo fibers, providing a foundation for further investigations into their adsorption behavior and potential applications in wastewater treatment.

3.1.4. SEM Analysis. In-depth insights into the structural modifications of bamboo fibers, pre and post-treatment with cetyltrimethylammonium bromide (CTAB), as well as subsequent dye loading with Reactive Blue 235 (RB235), were obtained through advanced surface characterization techniques, specifically scanning electron microscopy (SEM) and energy dispersive X-ray (EDX) analysis.

SEM images unveiled distinctive surface morphologies, highlighting the transformative impact of the CTAB treatment. Bamboo before treatment (BBT) displayed a pristine, smooth surface (Figure 4(a)), while bamboo after treatment (BAT) (Figure 4(b)) showcased a surface adorned with

numerous ridges and fissures, indicative of the surfactant's influence. The enhanced roughness of BAT underscores the successful modification induced by CTAB. Furthermore, the SEM image of Reactive Blue-loaded BAT (RB-BAT) (Figure 4(c)) provided visual confirmation of the dye molecules firmly adhering to the BAT surface. This observation is crucial, as it substantiates the adsorption capacity and efficiency of BAT in capturing and retaining dye molecules.

Energy dispersive X-ray (EDX) analysis delved into the elemental composition of BBT, BAT, and RB-BAT, shedding light on the molecular constituents present on the fiber surfaces. In the case of BBT (Figure 5(a)), the major elements were carbon and oxygen. Intriguingly, the surfaces of both BAT (Figure 5(b)) and RB-BAT (Figure 5(c)) exhibited the presence of bromine, signifying the incorporation of hexadecyltrimethylammonium bromide molecules during the treatment process. This result aligns with the expected outcome, as CTAB, a bromide-containing surfactant, was utilized in the modification. Additionally, the EDX analysis of RB-BAT (Figure 5(c)) revealed the existence of copper (Cu), sodium (Na), sulfur (S), and fluorine (F), elements

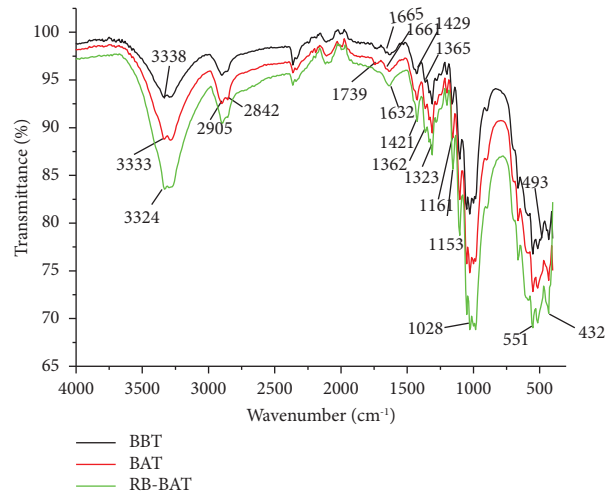


FIGURE 2: FT-IR spectra of BBT, BAT, and RB-BAT.

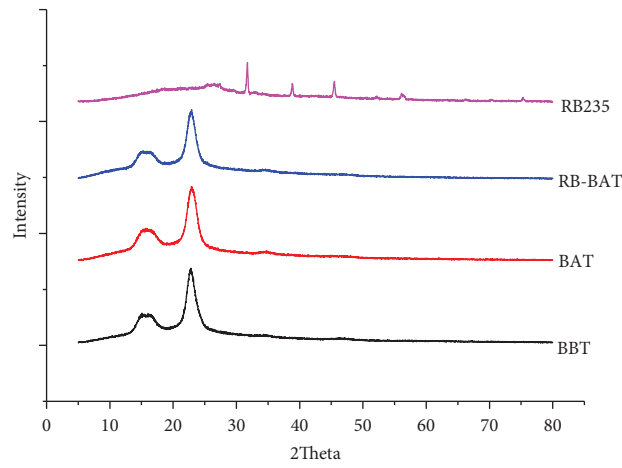


FIGURE 3: XRD spectra of BBT, BAT, RB-BAT, and RB235.

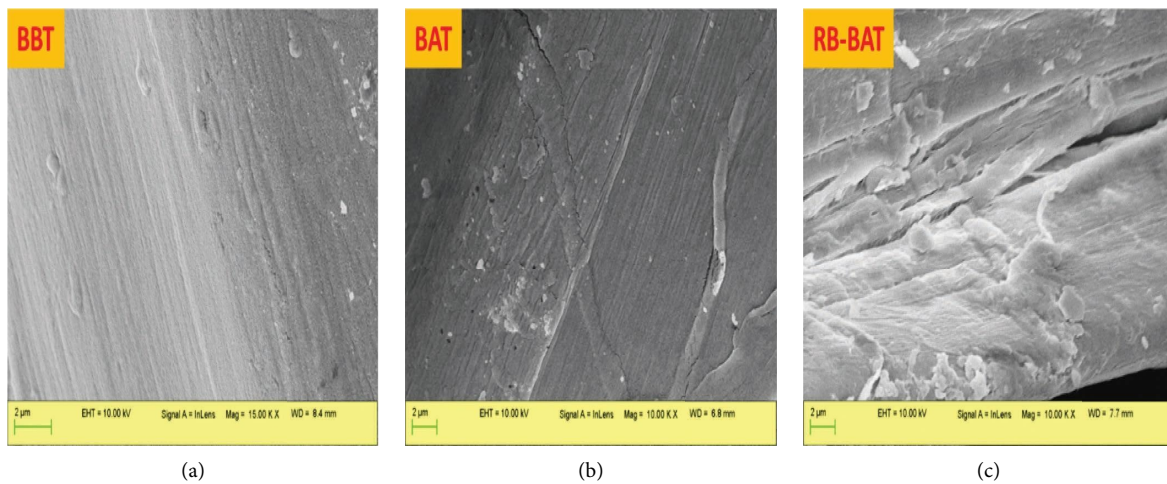


FIGURE 4: SEM images of (a) BBT, (b) BAT, and (c) RB-BAT.

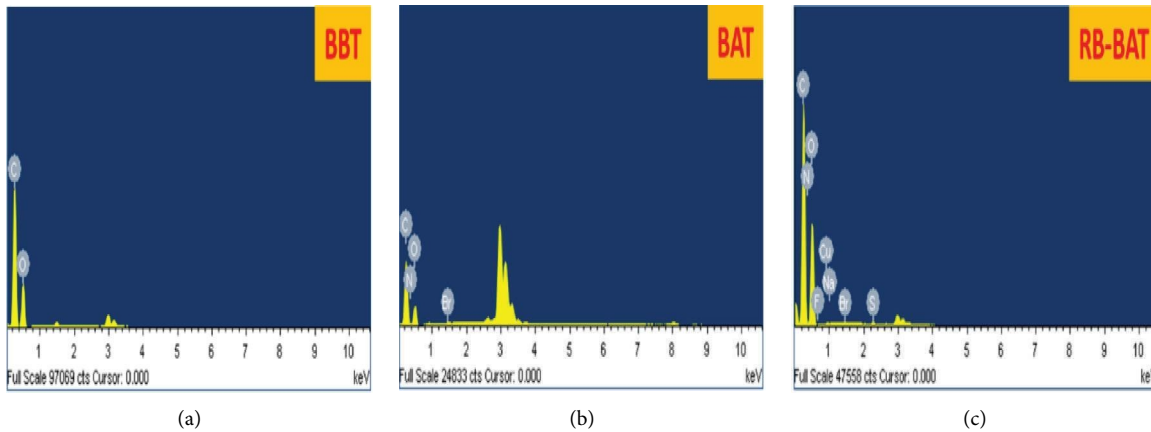


FIGURE 5: EDX of (a) BBT, (b) BAT, and (c) RB-BAT.

characteristic of Reactive Blue 235 dye. This corroborates the successful loading of the dye onto the BAT surface, reinforcing the material's potential as an effective adsorbent for dye removal in wastewater treatment.

In summary, the integrated SEM and EDX analyses provide a nuanced understanding of the structural and compositional changes brought about by the CTAB treatment and dye loading. These changes not only confirm the efficacy of BAT as an adsorbent but also lay the groundwork for a comprehensive assessment of its adsorption behavior and potential applications in sustainable wastewater treatment strategies.

3.1.5. TGA Analysis. Thermogravimetric analysis (TGA) was employed to gain a comprehensive understanding of the thermal stability of bamboo before treatment (BBT), bamboo after treatment (BAT), and Reactive Blue-loaded BAT (RB-BAT) under a nitrogen atmosphere. The TGA results, illustrated in Figure 6, delineate the intricate thermal degradation processes occurring within the bamboo fibers at varying temperature ranges.

The TGA curves exhibit three distinct stages of mass loss at temperature intervals of 25–320°C, 320–380°C, and 380–550°C. Each phase corresponds to specific thermal events, providing valuable insights into the thermal behavior of the materials.

In the initial stage, ranging from 25 to 320°C, the mass loss is attributed to the removal of water molecules from the adsorbent and the decomposition of low molecular weight organic compounds. This phase primarily addresses the elimination of moisture content within the materials.

The second phase, spanning 320 to 380°C, reveals a sharp decrease in mass. This is indicative of the degradation of the main hemicellulose skeleton present in BBT, BAT, and RB-BAT. The specific temperature range suggests the depolymerization of hemicellulose components, elucidating the thermal changes induced by CTAB treatment and dye loading.

The third phase, occurring between 380 and 550°C, signifies further decomposition. This stage involves the breakdown of cellulose and the 0.4% lignin components

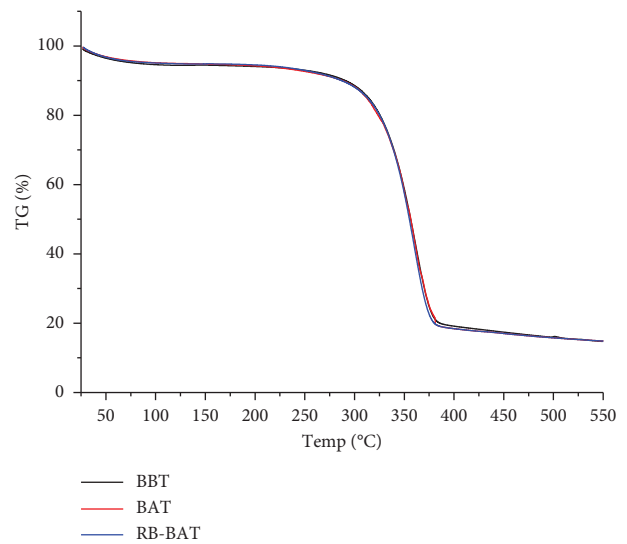


FIGURE 6: TGA of BBT, BAT, and RB-BAT.

present in BBT, BAT, and RB-BAT. The comprehensive decomposition process sheds light on the thermal stability of the materials across various temperature regimes.

The TGA analysis not only provides a qualitative assessment of the thermal stability of BBT, BAT, and RB-BAT but also offers quantitative data on the extent of mass loss during distinct temperature intervals. Understanding the thermal behavior is crucial for evaluating the materials' performance under varying environmental conditions, especially in potential applications involving thermal treatment or exposure to elevated temperatures. The multistage mass loss observed in the TGA curves contributes to a nuanced comprehension of the thermal dynamics within the bamboo fibers, enhancing our insights into their stability and suitability for diverse applications.

3.1.6. BET Analysis. The BET surface area, single-point adsorption total pore volume, and BET average pore width (calculated as $4V/A$ by BET) were extracted from the adsorption isotherms. For BAT, the BET surface area was determined to be $0.3944 \text{ m}^2/\text{g}$, the single-point adsorption

total pore volume was $2.746757 \text{ cm}^3/\text{g}$, and the BET average pore width stood at 278605.2840 \AA . In comparison, BBT exhibited a BET surface area of $0.0625 \text{ m}^2/\text{g}$, a single-point adsorption total pore volume of $3.266709 \text{ cm}^3/\text{g}$, and a BET average pore width of 2090973.1769 \AA .

The BET analysis offers crucial information regarding the porosity and surface area of the adsorbents, which are paramount factors influencing their adsorption capacity. The higher BET surface area of BAT ($0.3944 \text{ m}^2/\text{g}$) in contrast to BBT ($0.0625 \text{ m}^2/\text{g}$) indicates that the CTAB treatment led to an increase in the available surface for adsorption. This augmentation in surface area correlates with the structural changes observed in SEM analysis, where BAT exhibited a surface covered with ridges and fissures, enhancing its adsorption potential.

Additionally, the single-point adsorption total pore volume signifies the total volume of pores accessible for adsorption. BAT exhibited a lower pore volume ($2.746757 \text{ cm}^3/\text{g}$) compared to BBT ($3.266709 \text{ cm}^3/\text{g}$), suggesting that the surfactant treatment influenced the pore structure, potentially leading to a more selective adsorption process.

The BET average pore width provides information about the size of pores within the material. BAT displayed a smaller average pore width (278605.2840 \AA) compared to BBT (2090973.1769 \AA), indicating a more refined pore structure post-treatment.

In summary, the BET analysis enhances our understanding of the surface characteristics, porosity, and potential adsorption sites within BAT and BBT. These findings contribute to a comprehensive assessment of the adsorption behavior, aiding in the determination of the materials' suitability for specific environmental applications.

3.2. Effect of the Adsorbent Dose. The study delved into the influence of adsorbent dosage on the percentage of dye removal, shedding light on the optimal conditions for effective Reactive Blue 235 (RB235) removal. The outcomes of this investigation are illustrated in Figure 7, providing insights into the comparative performance of bamboo before treatment (BBT) and bamboo after treatment (BAT) under varying doses.

The graph portrays the dynamic relationship between the adsorbent dose and the efficiency of dye removal, specifically focusing on a dye concentration of 40 mg/L . Notably, the data reveal that the highest degree of dye removal is achieved with the utilization of 0.5 g of BAT for a 50 ml solution containing 40 mg/L RB235 dye.

Analyzing the findings from Figure 7, a clear trend emerges, highlighting the optimal dosage of $0.5 \text{ g}/50 \text{ ml}$ of dye solution (40 mg/L) for maximum dye removal. The superior performance of BAT compared to BBT underscores the significance of surfactant functionalization in enhancing the adsorption capacity of bamboo fibers. The initial negative charge of untreated bamboo fibers is effectively transformed into positive surface charges through surfactant treatment. This positive charge modification contributes to an improved affinity for reactive anionic dyes like RB235.

The observed trend not only provides practical insights for optimizing the adsorbent dosage in real-world applications but also substantiates the research hypothesis. The surfactant-functionalized bamboo fiber (BAT) demonstrates enhanced efficacy in dye removal compared to its untreated counterpart (BBT). The positive surface charges acquired during the surfactant treatment process play a pivotal role in augmenting the adsorption affinity for anionic dyes.

These findings are pivotal for designing efficient adsorption systems for textile effluent treatment. They offer a nuanced understanding of the adsorbent dose-response relationship, enabling the customization of treatment protocols for varying dye concentrations. Ultimately, this knowledge contributes to the development of sustainable and effective wastewater treatment strategies, aligning with the broader goals of environmental conservation.

3.3. Effect of pH. The investigation into the effect of pH on the adsorption of Reactive Blue 235 onto bamboo before treatment (BBT) and bamboo after treatment (BAT) provides critical insights into the interplay between solution chemistry, surface charge, and adsorption capacity. The experimental results, presented in Figure 8, elucidate the nuanced relationship between pH variations and the efficiency of dye removal in a 40 mg/L dye solution at 298 K .

The graph captures the dynamic response of dye removal percentage to alterations in pH, offering a comprehensive understanding of the pivotal role played by pH in influencing the adsorption process. Notably, the investigation utilized a dye solution concentration of 40 mg/L with an adsorbent dose of 0.5 g per 50 ml of the dye solution.

From Figure 8, a discernible pattern emerges, unveiling the sensitivity of dye removal to changes in pH. The percentage of dye removal exhibits an incremental trend as pH decreases from 8 to 2. Intriguingly, beyond a pH of 8, there is a gradual reduction in the percentage of dye removal.

The observed pH-dependent trend can be attributed to the intricate interplay between the chemistry of the dye solution and alterations in the surface charge of the adsorbent. At lower pH levels, the positively charged surface of the adsorbent, induced by surfactant treatment, facilitates electrostatic attraction with anionic dye molecules [90]. This favorable interaction contributes to the enhanced adsorption capacity observed. The affinity of RB235 for the BAT in an acidic medium is due to the anionic nature of the dye molecule which showed higher adsorption capacity in the medium [91].

Conversely, as pH increases beyond 8, the reduction in positive charge on the adsorbent surface diminishes the electrostatic attraction between the adsorbent and the anionic dye molecules. This diminishing affinity results in a gradual decline in the percentage of dye removal. The findings align with the established principle that pH significantly influences the surface charge of adsorbents, thereby modulating their adsorption capabilities.

In summary, the exploration of pH effects on dye adsorption not only substantiates the intricate dynamics at play but also provides valuable insights for optimizing the

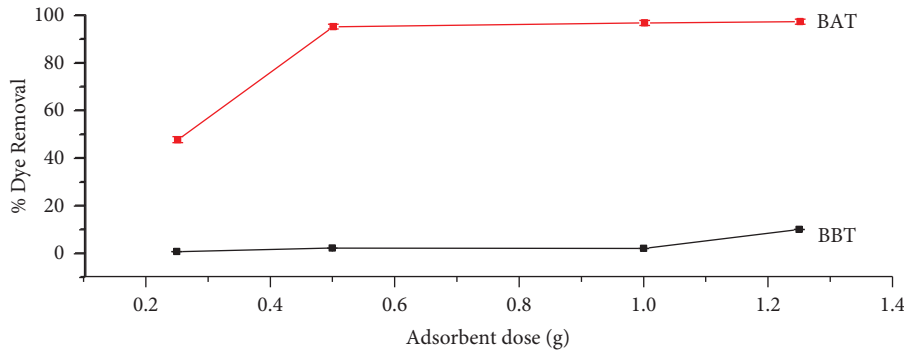


FIGURE 7: Effect of BBT and BAT dose on dye removal (conc. of dye solution, $C_o = 40$ mg/L, contact time = 40 min, and temperature = 298 K).

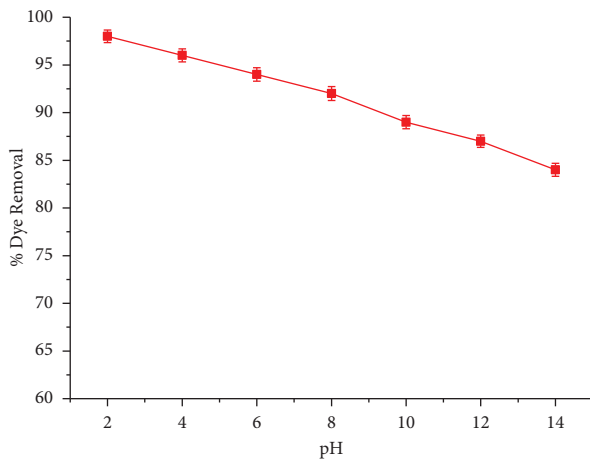


FIGURE 8: Effect of pH on adsorption of Reactive Blue 235 on BAT (conc. of dye solution, $C_o = 40$ mg/L, adsorbent dose = 0.5 g/50 ml of dye solution, contact time = 40 min, and temperature = 298 K).

pH conditions in practical applications. This knowledge is instrumental for tailoring effective and sustainable dye removal strategies in textile effluent treatment.

3.4. Effect of Contact Time. The investigation into the temporal dynamics of Reactive Blue 235 dye removal, employing both bamboo before treatment (BBT) and bamboo after treatment (BAT), unravels crucial insights into the time-dependent efficiency of the adsorption process. The experimental findings, depicted in Figure 9, illuminate the evolution of dye removal percentages with varying contact times, providing a comprehensive understanding of the optimal temporal conditions for efficient dye elimination in a 40 mg/L dye solution at 298 K.

This graph serves as a temporal roadmap, delineating the progression of dye removal percentages as the contact time between the adsorbents and the dye solution extends. The experimental parameters included an adsorbent dose of 0.5 g per 50 ml of the dye solution, maintaining a constant dye solution concentration at 40 mg/L.

Figure 9 vividly illustrates the direct correlation between contact time and the percentage of Reactive Blue 235 dye removal. As the contact time escalates from 0 minutes to 60 minutes, a steady increase in the percentage of dye

removal is observed. Notably, within the initial ten minutes of contact, BAT exhibits an exceptional performance, eliminating more than 80% of the dye.

The time-dependent nature of the adsorption process is evident in the observed trend. The initial phase of rapid dye removal can be attributed to the availability of vacant adsorption sites on the surface of BAT, enabling swift interactions with the dye molecules. As the contact time extends, more adsorption sites become engaged, contributing to the continuous increase in dye removal percentages.

The exceptional performance of BAT, surpassing 80% dye removal within ten minutes, underscores the effectiveness of surfactant-functionalized bamboo fibers. The surfactant treatment not only enhances the affinity for anionic dye molecules but also facilitates rapid adsorption kinetics.

Understanding the temporal dynamics of dye removal is pivotal for optimizing operational parameters in practical applications, ensuring resource-efficient and time-effective wastewater treatment strategies. These findings contribute to the design of sustainable and expeditious adsorption processes for textile effluent remediation.

3.5. Effect of Initial Concentration of Dye. The exploration of the intricate relationship between the initial concentration of Reactive Blue 235 dye and the quantity adsorbed unfolds in Figure 10 shedding light on the dynamic interplay influencing the adsorption process. This investigation, conducted with bamboo after treatment (BAT), scrutinizes the variations in dye adsorption ($\text{mg}\cdot\text{g}^{-1}$) in response to a diverse range of initial dye concentrations, spanning from 20 mg/L to 100 mg/L, at 298 K.

This graph serves as a visual representation of the evolving correlation between dye adsorption and varying initial dye concentrations, offering valuable insights into the underlying mechanisms at play during the adsorption process.

Figure 10 unveils a proportional relationship between the initial dye concentration and the quantity of dye adsorbed onto BAT. As the initial dye concentration escalates from 20 mg/L to 100 mg/L, there is a corresponding increase in the amount of dye adsorbed by the adsorbent.

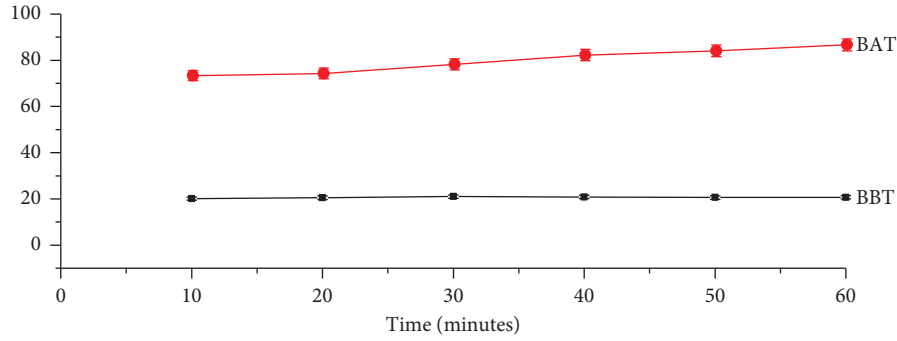


FIGURE 9: Effect of contact time on adsorption of Reactive Blue 235 onto BAT and BBT (adsorbent dose = 0.5 g/50 ml of dye solution, conc. of dye solution, $C_o = 40$ mg/L, and temperature = 298 K).

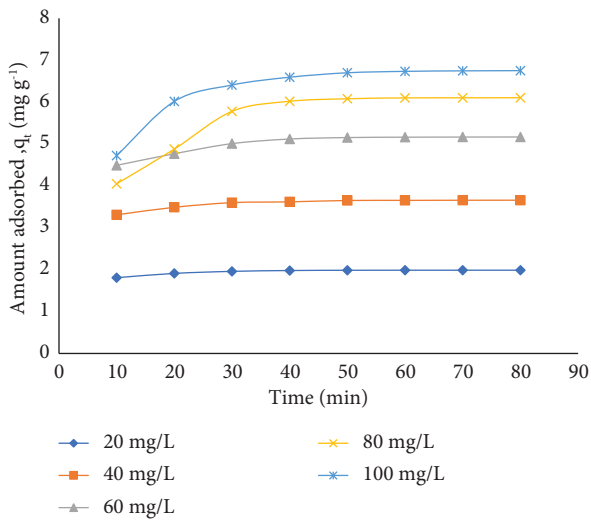


FIGURE 10: Effect of the contact time on Reactive Blue 235 adsorption at different initial concentrations of dye onto BAT at 298 K.

The observed correlation finds its roots in the principles of diffusion and concentration gradients. With an elevation in the initial dye concentration, a heightened diffusion of dye molecules from the solution onto the BAT surface is witnessed. This phenomenon is propelled by the development of a concentration gradient between the dye solution and the adsorbent (BAT), amplifying the driving force behind the adsorption process.

The concentration gradient acts as a compelling driving force, propelling a greater influx of dye molecules towards the adsorbent surface. Consequently, the adsorption capacity of BAT is maximized at higher initial dye concentrations.

Understanding the impact of initial dye concentration is pivotal for optimizing adsorption systems, especially in scenarios where varying dye concentrations are encountered in real-world applications. These findings provide a nuanced understanding of the concentration-driven dynamics, aiding in the design of efficient and adaptable adsorption processes for the treatment of textile effluents.

3.6. Adsorption Kinetic Study. Understanding the kinetics of the adsorption process is pivotal for unravelling the underlying mechanisms governing the efficiency and behavior of the adsorbent. In this study, both pseudo-first-order and pseudo-second-order models were employed to scrutinize the adsorption type, capacity, and rate of the system. The evaluation of these kinetic models was based on the determination of R^2 values, alongside a meticulous comparison between experimental values (q_e, exp) and calculated values (q_e, cal) of adsorption capacity. The model with the best fit was identified through this comprehensive analysis.

3.6.1. Pseudo-First-Order Reaction Kinetics. The pseudo-first-order kinetic model's linear form can be written as [92]

$$\log(q_e - q_t) = \log q_e - \frac{k_1 t}{2.303}, \quad (3)$$

where q_t ($\text{mg}\cdot\text{g}^{-1}$) and q_e ($\text{mg}\cdot\text{g}^{-1}$) are the quantity of adsorbed dye by BAT at time t (min) and equilibrium, respectively. k_1 (min^{-1}) is the pseudo-first-order rate constant.

The intercept and slope of the plot of $\log(q_e - q_t)$ versus t (Figure 11) yield the parameters q_e and k_1 , respectively.

Although the R^2 value obtained from pseudo-first order plot is significant, a notable disparity exists between the experimental q_e values and the calculated ones, as detailed in Table 1. These findings underscore that the pseudo-first-order model fails to accurately represent the kinetics of the adsorption process, prompting the exploration of alternative models to elucidate the dynamic behavior of Reactive Blue 235 adsorption onto BAT.

3.6.2. Pseudo-Second-Order Reaction Kinetics. In addition to the pseudo-first-order model, a comprehensive exploration of the adsorption kinetics involved the application of the pseudo-second-order kinetic model, represented by the following equation [93]:

$$\frac{t}{q_t} = \frac{1}{k_2 q_e^2} + \frac{t}{q_e}, \quad (4)$$

where k_2 ($\text{g}\cdot\text{mg}^{-1}\cdot\text{min}^{-1}$) is the rate constant of second-order reaction. The rate constant k_2 and q_e were determined from the intercept and slope, respectively, of the plots of t/q_t versus t (Figure 12).

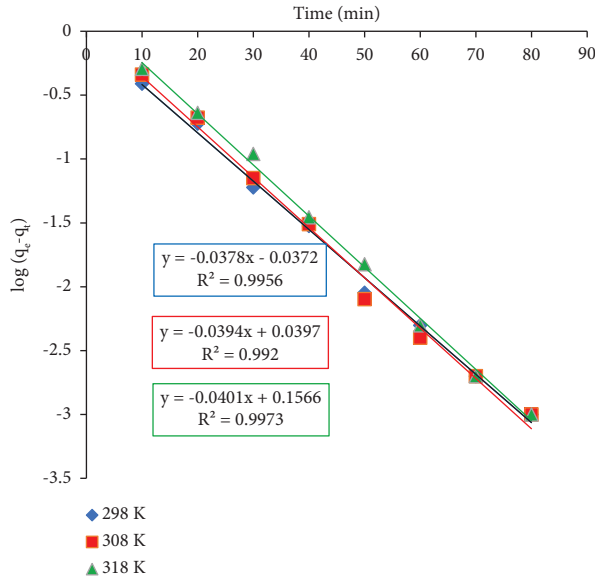


FIGURE 11: Pseudo-first-order linear plots for adsorption of Reactive Blue 235 on BAT at 298 K, 308 K, and 318 K.

The outcome of this analysis supports the conclusion that adsorption follows the pseudo-second-order kinetic model. This is evident from the high R^2 values, approximating 0.999 or 1, and the close agreement between the experimental q_e values and their calculated counterparts, as detailed in Table 1. This unequivocally demonstrates that the adsorption of Reactive Blue 235 onto BAT aligns closely with the pseudo-second-order kinetic model, providing a deeper understanding of the dynamic behavior of the adsorption process.

3.6.3. Intra-Particle Diffusion Model. In the quest to decipher the diffusion mechanism governing the adsorption, the intra-particle diffusion model proposed by Weber and Morris [94] was employed. The model is mathematically expressed as

$$q_t = k_i t^{1/2} + C_i, \quad (5)$$

where k_i is the intra-particle diffusion rate ($\text{mg}\cdot\text{g}^{-1}\cdot\text{min}^{-1/2}$).

If the only step in the adsorption process that limits rate is intra-particle diffusion, the plot of q_t versus $t^{1/2}$ should represent straight lines passing through origin. The rate constants C_i ($\text{mg}\cdot\text{g}^{-1}$) and k_i are determined from the intercept and slope of the regression line, respectively. C signifies the thickness of the boundary layer. The larger value of C signifies the larger effect of the boundary layer as indicated in Table 2.

It can be seen from the graph (Figure 13) that the plots of q_t versus $t^{1/2}$ are not passing through origin, this indicates a lower degree of boundary layer control, and it further showed that just intra-particle diffusion was not the rate-limiting step, rather there might be some other processes also controlling the adsorption rate. The boundary layer effect increases as temperature rises, as shown by the C values.

3.6.4. Boyd Plot. To find out the actual rate-controlling step of the adsorption, the acquired data were additionally investigated using the kinetic expression specified by Boyd et al. [95]. This model was used to distinguish between film diffusion and particle diffusion. Particle diffusion happens when a transfer of the adsorbate occurs within the pores of the adsorbent (internal transport > external transport), and film diffusion happens when the transfer of adsorbate occurs on the surface of the adsorbent (internal transport < external transport) [96].

$$F = 1 - \frac{6}{\pi^2} \exp(-Bt), \quad (6)$$

where F is the fractional achievement of equilibrium at a time " t " and Bt is a mathematical function of F . F (fractional attainment) is calculated by using the following equation:

$$F = \frac{q_t}{q_e}. \quad (7)$$

Here, q_t ($\text{mg}\cdot\text{g}^{-1}$) is the quantity of dye adsorbed after time t and q_e ($\text{mg}\cdot\text{g}^{-1}$) is the quantity of dye adsorbed at equilibrium. Applying (6) into (5), (5) becomes

$$Bt = -0.4977 - \ln\left(1 - \frac{q_t}{q_e}\right). \quad (8)$$

The adsorption rate for the particle and film diffusion was calculated with the help of Bt versus time (t) plot (Figure 14). If Bt versus t plot gives straight line that passes through the origin, then adsorption is said to be presided over by a particle-diffusion mechanism (transfer of the adsorbate within the pores of the adsorbent), or else presided over by film diffusion (transfer of adsorbate to surface of adsorbent). Figure 14 displays that the adsorption process in the present study is a film diffusion mechanism as the Bt versus t plot is not passing through the origin.

3.6.5. Elovich Model. This model is generally used to interpret the adsorption kinetics. It helps in successfully describing the pseudo-second-order kinetics supposing that the surface is energetically heterogenous. It is generally expressed as [97]

$$q_t = \frac{1}{\beta} \ln(\alpha\beta) + \frac{1}{\beta} \ln t, \quad (9)$$

where α and β are the initial adsorption rate ($\text{mg}\cdot\text{g}^{-1}$) and desorption constant ($\text{g}\cdot\text{mg}^{-1}$), respectively. q_t ($\text{mg}\cdot\text{g}^{-1}$) is the quantity of the dye adsorbed at time t (min). By plotting q_t versus $\ln t$ (Figure 15), the plot's slope and intercept can be used to determine the values of α and β . Table 3 lists the values of α and β at different temperatures.

3.6.6. Bangham's Model. The adsorption was assessed using Bangham's equation to be as pore diffusion controlled. Bangham equation is generally expressed as [98]

TABLE 1: Comparison of pseudo-first-order and pseudo-second-order kinetic models at various temperatures for the adsorption of Reactive Blue 235 on BAT.

Temperature (K)	Pseudo-first-order kinetic model				Pseudo-second-order kinetic model			
	q_e (exp) ($\text{mg}\cdot\text{g}^{-1}$)	q_e (cal) ($\text{mg}\cdot\text{g}^{-1}$)	K_1 (min^{-1})	R^2	q_e (exp) ($\text{mg}\cdot\text{g}^{-1}$)	q_e (cal) ($\text{mg}\cdot\text{g}^{-1}$)	K_2 ($\text{g}\cdot\text{mg}^{-1}\cdot\text{min}^{-1}$)	R^2
298	3.7	0.918	0.087	0.996	3.7	3.77	0.216	1
308	3.811	1.096	0.091	0.992	3.811	3.89	0.185	0.9999
318	3.91	1.434	0.092	0.997	3.91	4	0.157	0.9999

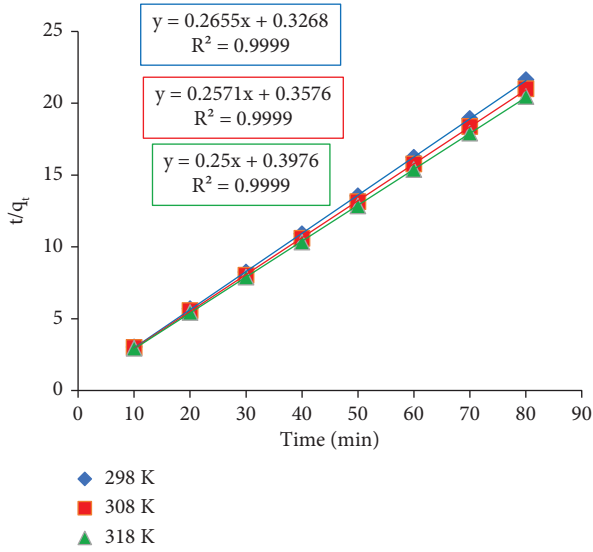


FIGURE 12: Pseudo-second-order linear plots for adsorption of Reactive Blue 235 on BAT at 298 K, 308 K, and 318 K.

TABLE 2: Comparison of C_i and K_i values at various temperatures.

Temperature (K)	C_i	K_i	R^2
298	3.218	0.0614	0.78
308	3.250	0.0717	0.7703
318	3.280	0.0802	0.7954

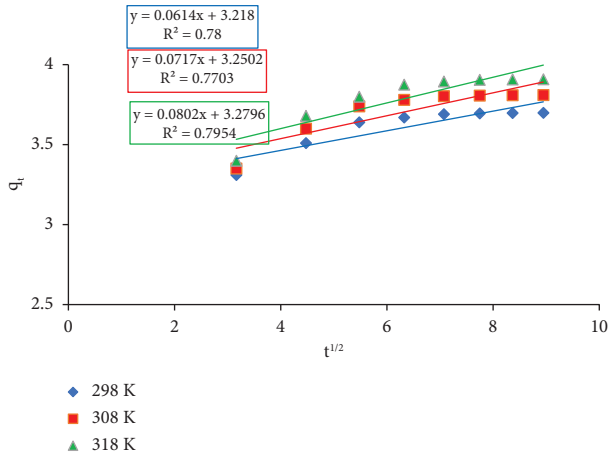


FIGURE 13: Weber-Morris intra-particle diffusion model for the adsorption of Reactive Blue 235 on BAT (conc. of dye solution = 40 mg/L and adsorbent dose = 0.5 g/50 ml).

$$\text{Log} \left[\log \left(\frac{C_o}{C_o - q_t m} \right) \right] = \log \left(\frac{k_o m}{2.303V} \right) + B \log t. \quad (10)$$

Here, C_o is the initial dye concentration in solution (mg/L). V is the volume of solution (ml), m is the weight of the adsorbent per litre of solution (g/L), q_t ($\text{mg}\cdot\text{g}^{-1}$) is the quantity of adsorbed dye at time t , and $B(<1)$ and k_o are constants, discussed in Table 4. An increase in temperature

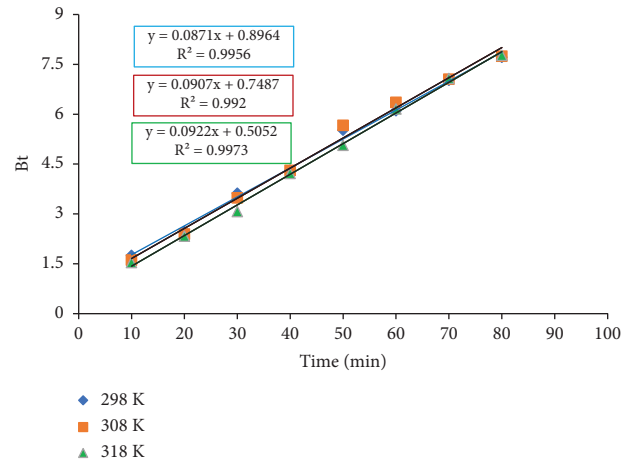


FIGURE 14: Boyd's plot for the adsorption of Reactive Blue 235 on BAT (conc. of dye solution = 40 mg/L and adsorbent dose = 0.5 g/50 ml).

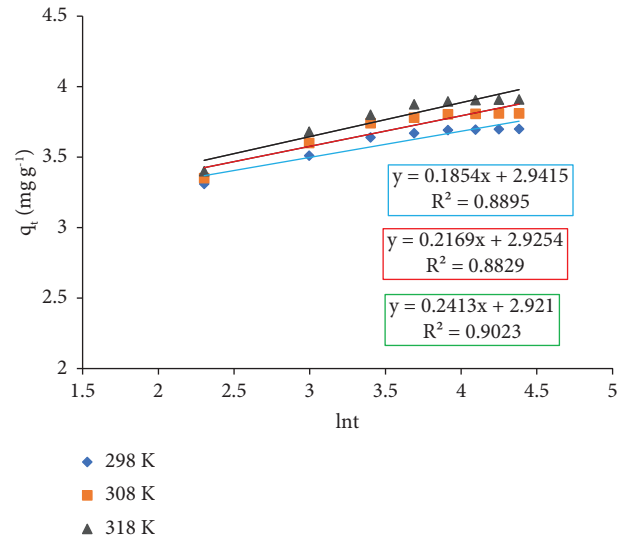


FIGURE 15: Elovich model for adsorption of Reactive Blue 235 on BAT (conc. of the dye solution = 40 mg/L and adsorbent dose = 0.5 g/50 ml).

TABLE 3: Comparison of α and β values at various temperatures.

Temperature (K)	α	β	R^2
298	1440263.937	5.393743258	0.89
308	156208.9072	4.61041955	0.883
318	43629.92005	4.144219	0.902

was found to result in an increase in the values of constants B and k_o .

Double logarithmic plot obtained from equation (10) did not produce adequate linear curves for the adsorption of Reactive Blue 235 onto BAT. This shows that the diffusion of adsorbents into the pores of the sorbent was not the only rate-controlling step (Figure 16). Therefore, the removal of dye molecules using BAT as adsorbent may involve both the pore and film diffusion mechanism, albeit to varying degrees.

TABLE 4: Comparison of B and k_0 values at various temperatures.

Temperature (K)	B	K_0	R^2
298	0.189	0.0044	0.91
308	0.253	0.0049	0.92
318	0.347	0.0059	0.96

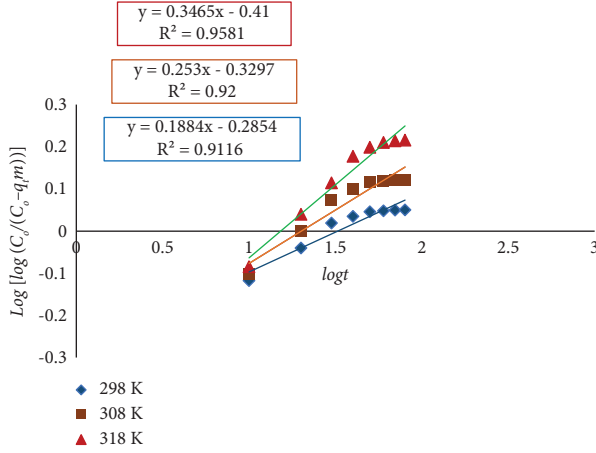


FIGURE 16: Bangham's model for adsorption of Reactive Blue 235 on BAT (conc. of the dye solution = 40 mg/L and dose of adsorbent = 0.5 g/50 ml).

3.7. *Adsorption Isotherms.* To compare and forecast the adsorbent's adsorption performance, adsorption isotherm data modelling is required. The practical design and operation of adsorption depend on the correlation between experimental results and the adsorption model, which can aid in understanding the mechanisms of adsorption and the heterogeneity of the surface of the adsorbent.

3.7.1. *Langmuir Isotherm.* According to the Langmuir adsorption isotherm, the adsorbate molecules develop a monolayer on the adsorbent's surface. Adsorbate adsorption at a specific location occurs regardless of whether adsorbate is present at nearby sites. The most popular and straightforward explanation of the adsorption process is Langmuir's model, which ignores the change in adsorption energy. In linearized form, a representation of Langmuir's model is as follows [99]:

$$\frac{C_e}{q_e} = \frac{1}{K_L q_m} + \frac{1}{q_m} \times C_e, \quad (11)$$

where C_e is the dye concentration (mg/L) at equilibrium and q_e is the adsorption capacity at equilibrium ($\text{mg}\cdot\text{g}^{-1}$). The maximum monolayer adsorption capacity is indicated by the constant q_m ($\text{mg}\cdot\text{g}^{-1}$), which is dependent on the number of adsorption sites. K_L is correlated with the adsorbate's affinity for the binding sites. Table 5 illustrates the values of q_m ($\text{mg}\cdot\text{g}^{-1}$) and K_L , which were determined by analyzing the slope and intercept of the plots C_e/q_e versus C_e (Figure 17).

R_L , a dimensionless separation factor, can be used to express the main features of the Langmuir equation, which is defined by the following equation [100]:

$$R_L = \frac{1}{(1 + K_L C_0)}, \quad (12)$$

where C_0 is the initial concentration of dye (mg/L). The adsorption process's nature is indicated by the value of parameter R_L , as indicated in Table 6.

It is evident from the data in Table 5 that as the temperature has increased, so too have the values of the constants K_L and q_m . The explanation for this could be that as the temperature rises, the dye's kinetic energy rises as well, increasing the dye ions' mobility. Consequently, there was a greater likelihood of the dye being adsorbed onto the adsorbent, leading to an increase in its q_m .

3.7.2. *Freundlich Isotherm.* The sorbent's surface heterogeneity is described by the empirical equation known as the Freundlich isotherm model. It takes into account interactions between molecules that are absorbed as well as multiple adsorption layers with an uneven distribution of active site energy [101]. In linearized form, Freundlich's model is represented as

$$\ln q_e = \ln K_F + \frac{1}{n} \ln C_e, \quad (13)$$

where q_e is the quantity of adsorbed dye per unit of adsorbent ($\text{mg}\cdot\text{g}^{-1}$) at equilibrium and C_e is the dye concentration in solution at equilibrium (mg/L). The Freundlich adsorption isotherm constants regarding the adsorption intensity and capacity are denoted by n and K_F , respectively. Through the intercept and slope obtained from the linear plot of $\ln q_e$ versus $\ln C_e$ (Figure 18), the values of n and K_F were computed and are shown in Table 7. This model's favorable adsorption can be described as follows: adsorption is favorable if n is greater than unity.

It is indicated that the adsorption conditions are favorable since n is greater than 1. Higher temperatures appeared to favor the removal of dye Reactive Blue 235 by this adsorbent, as indicated by the K_F values increasing with temperature. An increasing trend with the temperature further suggested that this adsorption phenomenon is endothermic. Furthermore, for the adsorption of the dye Reactive Blue 235, the K_F values displayed the identical temperature dependence pattern as q_m in the Langmuir model.

3.7.3. *Temkin Isotherm.* The Temkin isotherm includes a factor that evidently accounts for the interactions between the adsorbent and the adsorbate. This isotherm is predicated on the following assumptions: (i) all molecules in the layer experience a linear decrease in heat of adsorption with increasing coverage due to adsorbent-adsorbate interactions; and (ii) up to a certain maximum binding energy, an even distribution of the binding energies is the characteristic of adsorption [102, 103]. Temkin's isotherm model thus suggests that the adsorption energy decreases linearly with surface coverage due to interactions between the adsorbent and adsorbate. This isotherm's linear form is provided by

TABLE 5: Langmuir constants at different temperatures.

Temperature (K)	Reactive Blue 235 concentration (mg/L)	R_L	K_L (L/mg)	q_m (mg·g ⁻¹)	R^2
298	20	0.09	0.534	7.00	0.99
	40	0.05			
	60	0.03			
	80	0.024			
	100	0.019			
308	20	0.08	0.664	7.21	0.99
	40	0.04			
	60	0.03			
	80	0.02			
	100	0.02			
318	20	0.09	0.861	7.36	0.99
	40	0.05			
	60	0.03			
	80	0.03			
	100	0.02			

The obtained separation factor values, R_L , at 298 K, 308 K, and 318 K range from 0.02 to 0.09, demonstrating the present adsorption process's favorability.

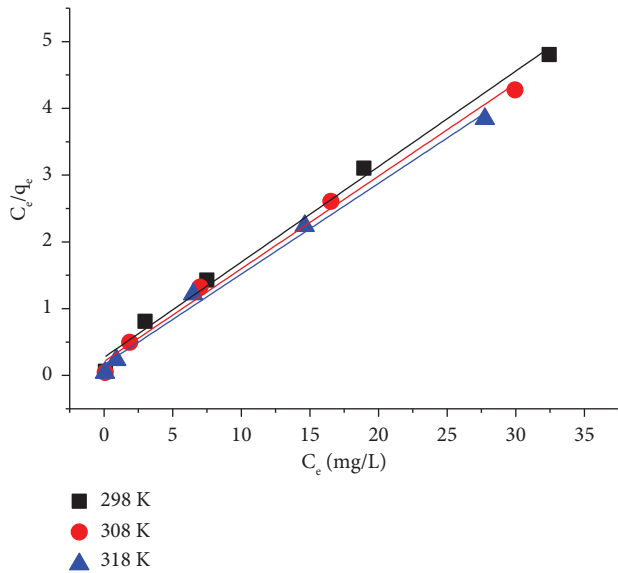


FIGURE 17: Plot of C_e/q_e versus C_e for the adsorption of Reactive Blue 235 onto BAT at 298 K, 308 K, and 318 K.

TABLE 6: Relation between R_L values and type of adsorption.

Value of R_L	Type of adsorption process
$R_L = 0$	Irreversible adsorption
$R_L = 1$	Linear adsorption
$0 < R_L < 1$	Favorable adsorption
$R_L > 1$	Unfavorable adsorption

$$q_e = B_1 \ln k_T + B_1 \ln C_e, \quad (14)$$

where $B_1 = RT/b$.

Plotting q_e against $\ln C_e$ (Figure 19) aids in determining isotherm's constants k_T and B_1 given in Table 8. The heat of adsorption is represented by B_1 , whereas maximum binding

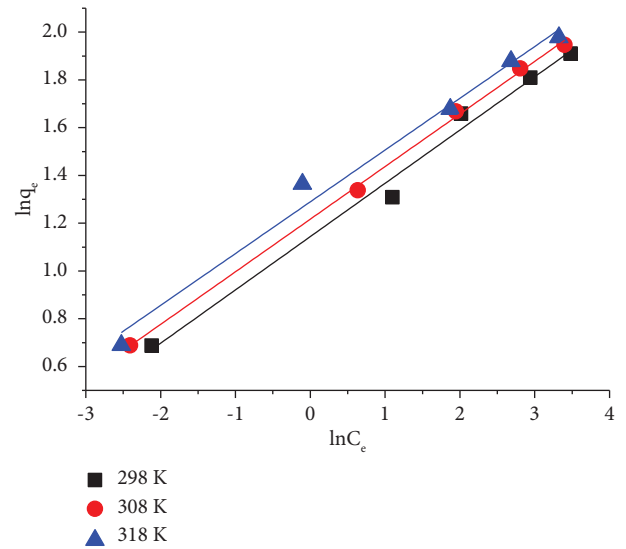


FIGURE 18: Plot of $\ln q_e$ versus $\ln C_e$ for adsorption of Reactive Blue 235 onto BAT at 298 K, 308 K, and 318 K.

TABLE 7: Freundlich's constants for Reactive Blue 235 adsorption on BAT at various temperatures.

Temperature (K)	K_F (mg·g ⁻¹) (L·mg ⁻¹) ^{1/n}	n	R^2
298	3.14	4.482	0.99
308	3.38	4.541	0.99
318	3.63	4.615	0.98

energy's accompanying equilibrium binding constant is k_T (L/mg) [103].

T represents the absolute temperature (K) and R is the gas's constant (8.314 J/mol K).

3.7.4. *Dubinin-Radushkevich (DR) Isotherm.* Due to its assumption of neither a homogeneous surface nor a fixed sorption potential, the Dubinin-Radushkevich (DR)

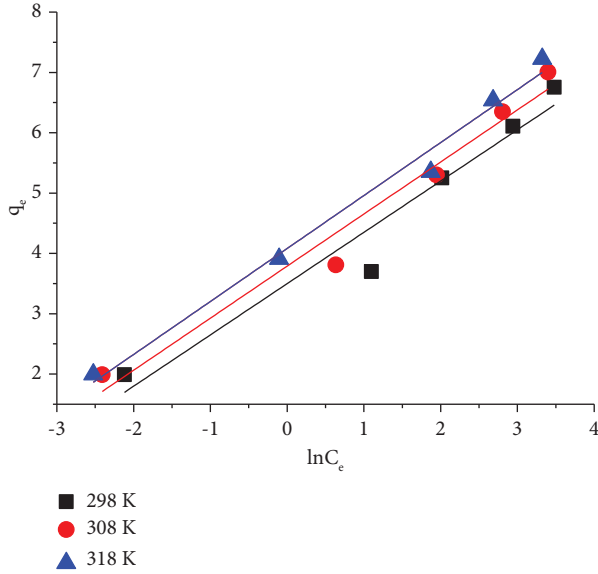


FIGURE 19: Plot of q_e against $\ln C_e$ for the Reactive Blue 235 adsorption onto BAT at 298 K, 308 K, and 318 K.

TABLE 8: Temkin constants for RB235 adsorption on BAT at different temperatures.

Temperature (K)	K_T (L/mg)	B_1	R^2
298	61.29	0.850	0.935
308	80.70	0.863	0.961
318	104.43	0.878	0.983

equilibrium model tends to be more general than the Langmuir isotherm [104]. In order to differentiate between the physical and chemical forms of adsorption, the DR model was proposed in the vicinity of the adsorbent surface within the adsorption space. The DR isotherm presumes that monolayer adsorption occurs in the adsorbent's micropores [105].

This isotherm is represented as

$$q_e = q_s \exp(-B\epsilon^2). \quad (15)$$

The linear form is as follows [27]:

$$\ln q_e = \ln q_s - B\epsilon^2, \quad (16)$$

where DR constant, q_s , is the theoretical saturation capacity of adsorbent ($\text{mg}\cdot\text{g}^{-1}$), B is a constant related to adsorption energy, and ϵ is the Polanyi potential (kJ/mol) and can be represented as

$$\epsilon = RT \ln \left(1 + \frac{1}{C_e} \right). \quad (17)$$

The constant B gives the average adsorption energy when adsorbate (dye molecules) is transferred to the surface of the adsorbent (BAT) from the dye solution and can be calculated using the following equation:

$$E = \frac{1}{(2B)^{1/2}}, \quad (18)$$

where R is the gas constant (8.314 J/mol K) and T is the absolute temperature.

Figure 20 displays a linear plot of $\ln q_e$ versus ϵ^2 for the dye Reactive Blue 235 at 298, 308, and 318 K for the Dubinin and Radushkevich (DR) method.

Plotting $\ln q_e$ versus ϵ^2 yields the values of B and q_s ($\text{mg}\cdot\text{g}^{-1}$), which can be found by analyzing its slope and intercept. The maximum quantity of adsorbate which is able to be adsorbed on the adsorbent is indicated by the constant q_s ($\text{mg}\cdot\text{g}^{-1}$). The DR constants calculated for Reactive Blue 235 adsorption on BAT at 298, 308, and 318 K are provided in Table 9. One can identify the type of adsorption by calculating the mean adsorption energy using the DR isotherm, i.e., it is chemisorption or physisorption. The magnitude of E in the context of physisorption varies from 1 to 8 kJ/mol, whereas if the value of E is greater than 8 kJ/mol, then it is said to be chemisorption. The current system's value of E indicates that Reactive Blue 235 is adsorbing on BAT in a physical manner.

The value of the maximum adsorption capacity of BAT determined from the Langmuir model ($q_m = 7.36 \text{ mg}\cdot\text{g}^{-1}$) at 318 K was found to be higher than that of the DR model ($q_s = 5.76 \text{ mg}\cdot\text{g}^{-1}$), indicating that BAT has a notable quantity of active sites.

The maximum uptake by a monolayer on the adsorbent surface is represented by q_m in the Langmuir model, whereas q_s in the DR model denotes the maximum uptake as a result of pore filling rather than monolayer adsorption. As a result, the two quantities are basically different, which accounts for the different values found when the two models are fitted to the experimental data. It appears that the DR model is less suitable for explaining our data, given that the Langmuir model fits the data better [106].

3.8. Adsorption Thermodynamics. Temperature-dependent adsorption of Reactive Blue 235 on BAT has also been revealed. For this purpose, the thermodynamic parameters like standard free energy change (ΔG^*), standard enthalpy change (ΔH^*), and standard entropy change (ΔS^*) are determined using the given equations [105]:

$$\begin{aligned} \Delta G^* &= -RT \ln K_c, \\ \Delta G^* &= \Delta H^* - T\Delta S^*. \end{aligned} \quad (19)$$

From equations (16) and (17), we get

$$\ln K_c = -\frac{\Delta H^*}{RT} + \frac{\Delta S^*}{R}, \quad (20)$$

where R (8.314 J/mol/K) is the universal gas constant, T (K) is the solution temperature in kelvin, and K_c (L/g) is the equilibrium constant. ΔH and ΔS can be computed using the slope and intercept of the graph between $\ln K_c$ and $1/T$ (Figure 21) [107]. Table 10 displays values for each thermodynamics parameter. The table shows that ΔG varies

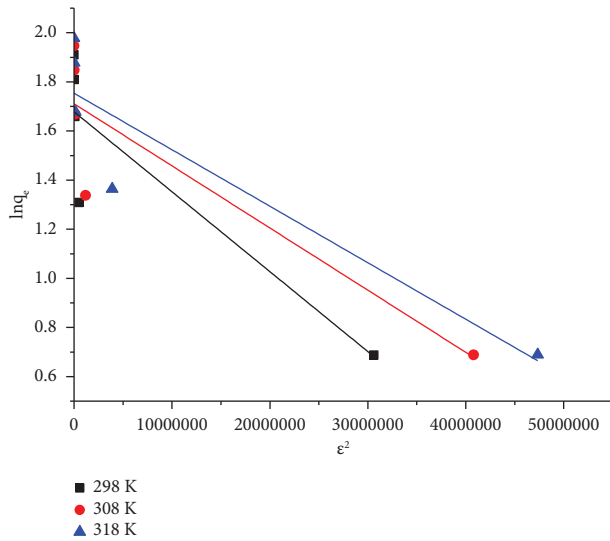


FIGURE 20: Plot of $\ln q_e$ versus ε^2 for the adsorption of Reactive Blue 235 onto BAT at 298 K, 308 K, and 318 K.

TABLE 9: Values of q_s and E at various temperatures.

Temperature (K)	q_s (mg·g ⁻¹)	E (kJ/mol)	R^2
298	5.36	3.92	0.73
308	5.53	4.44	0.75
318	5.76	4.66	0.80

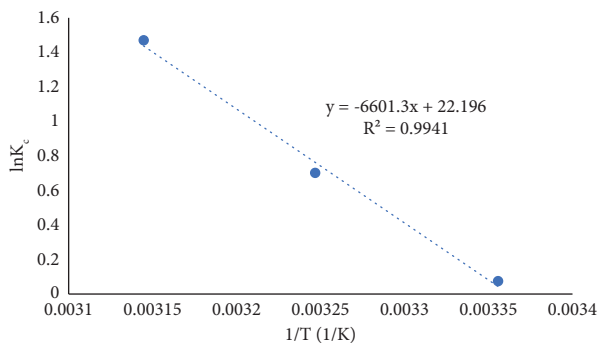


FIGURE 21: Plot of $\ln K_c$ versus $1/T$ for the adsorption of Reactive Blue 235 onto BAT.

TABLE 10: Thermodynamic parameters for RB235 adsorption onto BAT.

Temperature (K)	ΔG (kJ/mol)	ΔH (kJ/mol)	ΔS (J/mol/K)
298	-0.183		
308	-1.796	54.88	184.54
318	-3.884		

from -0.183 to -3.884 kJ/mol on increasing temperature from 298 K to 318 K. At all temperatures, ΔG is negative, which shows that Reactive Blue 235 can adsorb spontaneously and successfully on BAT. At elevated temperatures, the adsorption appears more favorable, as indicated by the progressively increasing negative values of ΔG with temperature [108–110]. This could be possible because a rise in

temperature causes the dye molecules' mobility in the solution to increase and thus the affinity of dye towards BAT is higher at high temperatures.

An endothermic adsorption phenomenon is suggested by a positive value of ΔH . The sorption type may also be inferred from the magnitude of ΔH . The heat produced by physical adsorption is 2.1–20.9 kJ/mol, the same as the heat produced by condensation, whereas the typical range for the heat of chemisorption is 80–200 kJ/mol. Therefore, rather than being solely the result of a physical or chemical adsorption process, it appears that this adsorption can be assigned to a physicochemical adsorption process, as seen from ΔH value given in Table 10 [111, 112].

Here, ΔS is positive, which signifies that entropy is driving the process of adsorption. During the adsorption process, a positive value of entropy change (ΔS) indicates a rise in disorder at the solid/liquid interface [113].

3.9. Adsorption Mechanism. In this section, the mechanism of RB235 dye uptake by BAT is discussed based on the characterization, kinetics, and isotherm study.

A possible adsorption mechanism of RB235 dye onto BAT is illustrated in Figure 22.

The RB235 dye could react with oxygen-containing functional groups including hydroxyl and carbonyl on the surface of BAT as suggested by FT-IR. The adsorption of RB235 dye on BAT followed the chemisorption type mechanism as demonstrated by the pseudo-second-order kinetic model (Figure 12) included in this investigation. The homogeneous kind of adsorption between RB235 and BAT was verified using the Langmuir adsorption isotherm (Figure 17) while the Dubinin–Radushkevich (DR) isotherm revealed the value of E varying from 3.92 to 4.66 kJ/mol which is in between 1 and 8 kJ/mol suggesting that Reactive Blue 235 is physically adsorbing on BAT. Prior research has established the simultaneous or synchronous existence of both processes, such as chemical and physical adsorption [114].

3.10. Removal of Dyes Using Synthetic Effluent. According to the adsorption data (kinetic and equilibrium), BAT was efficient in removing Reactive Blue 235 from aqueous solution, indicating that this could also be used to treat real effluents. For this, the real effluent was generated in the lab. To prepare the real textile effluent on a laboratory scale, the dyeing bath was prepared for cotton substrate. The shade percentage was taken as 1% using Reactive Blue 235 [115]. The soaping of dyed substrate was also carried out using nonionic detergent. The effluent was collected at four stages: (a) the used or exhausted dye bath; (b) rinsing; (c) soaping; and (d) final mixture of all the three types of effluents. These four effluents were studied separately as well as a combined effluent of these four stages was also studied regarding removal of dyes from these effluents using BAT adsorbent.

The %removal of dye from effluent was evaluated from UV-visible spectra of untreated and treated effluents (Figure 23).

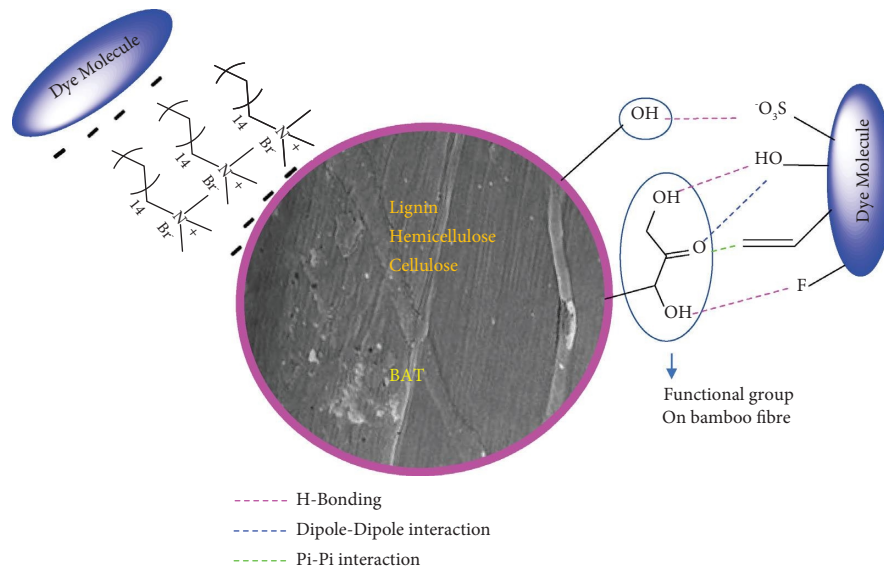


FIGURE 22: Proposed mechanism of adsorption of RB235 dye on adsorbent surface.

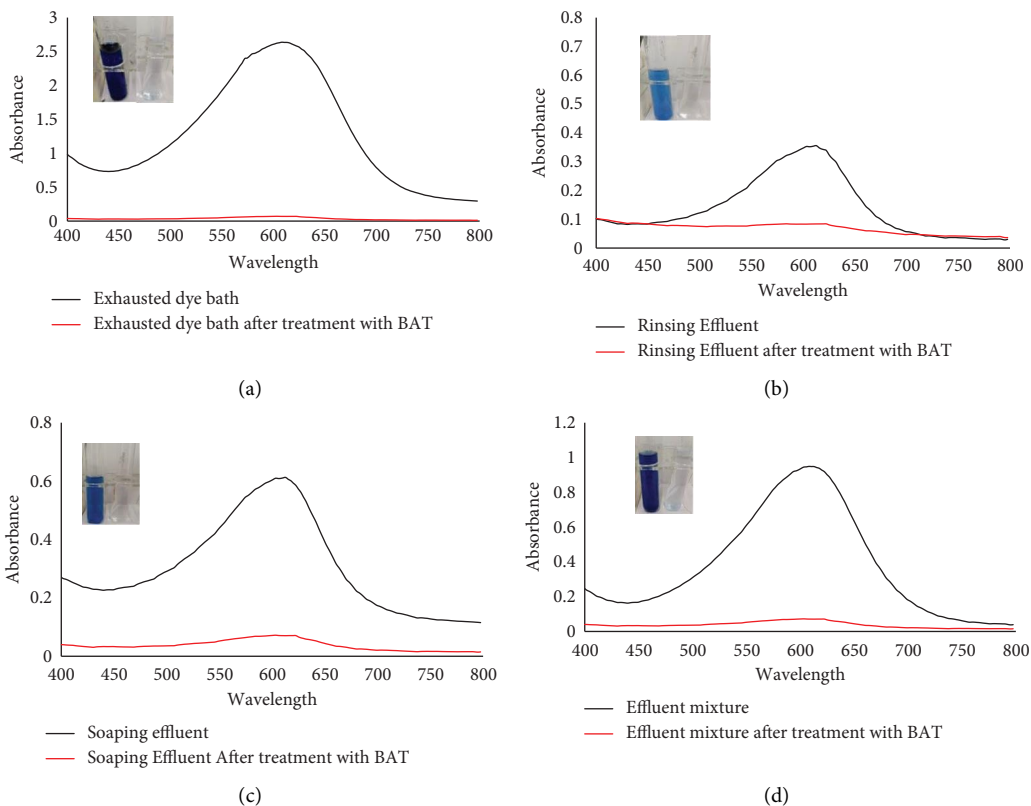


FIGURE 23: Adsorption of synthetic dye effluent collected at four stages a) exhausted dye bath b) rinsing effluent c) soaping effluent and d) final mixture of all the three types of effluents using BAT as adsorbent.

From the absorbance study, it was found that about 95% of dye was removed from real effluent using BAT as an adsorbent.

The K/S values, color images, color fastness, and light fastness of adsorbent and dye loaded adsorbent were also calculated using Datacolor 200M (given in Tables 11 and 12).

The K/S versus wavelength plot obtained from Datacolor 200M is shown in Figure 24.

3.11. Variables Controlling the Price of Reactive Blue 235 Adsorption on BAT. To maintain the sustainable utilization of the proposed method of the removal of the dye, it is very

TABLE 11: Color images and K/S values of various stages of adsorbent.

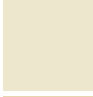


S.No.	Various stages of adsorbent	Color images	K/S values at 620 nm
1	BBT		0.06
2	BAT		0.07
3	RB-BAT		1.45

TABLE 12: Color fastness of the BAT sample loaded with dye RB235.

Sample	Change in color	SCA	BUC	Color staining				Light fastness
				N	P	A	WW	
RB-BAT	3-4	4	4-5	4	4	4	4	3-4

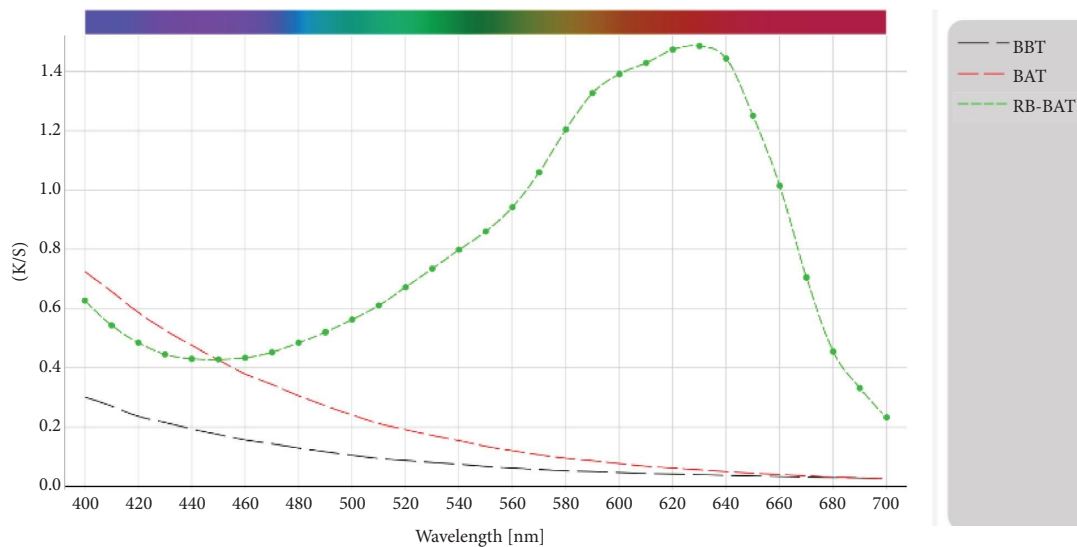


FIGURE 24: Plot of K/S versus wavelength obtained from Datacolor 200M.

much required to calculate the tentative overall execution cost. The overall execution cost was minimal. Along with the removal of the dye, the overall execution cost was also determined. It is found that the execution cost is minimal because of the minimum use of chemical amount and the low cost of adsorbent [116].

The execution cost is primarily determined by the following factors.

3.11.1. Adsorbent Cost (A). As the bamboo waste used in our study is easily available, its price is very low in comparison to other available adsorbents. The adsorbent costs nearly Rs. 5 per kg from a nearby supplier. 10 g of adsorbent is needed for removing dye from 1 litre of 40 mg/L dye solution. Thus, it will cost Rs. 0.05 per litre of colored solution.

3.11.2. Processing Cost (B). Surfactant CTAB is used for modifying the bamboo fibers which costs near about Rs. 950 per kg. For modifying 10 g of adsorbent, 0.57 g of CTAB is used. Thus, this step will cost Rs. 0.5415 per litre of dye solution (40 mg/L). Apart from this, the tentative cost of electricity consumed for drying the adsorbent and shaking the adsorbent after surface modification with CTAB has been estimated to be Rs. 2.03 Per litre of dye solution.

3.11.3. Batch Operation Cost (C). The continuous stirring is required for each batch operation (dye removal). To run a single batch, 40 minutes is required which requires a very small amount of electrical energy. The cost of this step is almost Rs. 1.45 per litre of dye solution.

TABLE 13: Comparing bamboo adsorbent with other reported adsorbents for removal of Reactive Blue 235 dye.

Adsorbent	Concentration of adsorbent used (g/L)	Contact time (minutes)	Initial dye concentration (mg/L)	Percentage dye removal (%)	References
Red-mud derived biologically synthesized iron nanoparticles (bRMINP)	1.5	240	10	98.75	[117]
Red-mud derived chemically synthesized iron nanoparticles (cRMINP)	1.5	240	10	88.88	[117]
CTAB-treated bamboo fibers (BAT)	10	40	40	94	Present study

So, the overall execution cost = adsorbent cost (A) + processing cost (B) + batch operation cost (C).

=Rs. (0.05 + 0.5415 + 2.03 + 1.45) per litre of dye solution.

=Rs. 4.0715 per litre of dye solution.

The best thing about the overall execution cost obtained is that with the increase in amount of dye solution (to be treated), the value of processing cost as well as batch operation cost will not be highly increased. The adsorbent cost will only be slightly increased.

Simultaneously, the color values (K/S values) and fastness properties of the used adsorbents have been studied. The K/S value showed that the maximum amount of the dye present in the effluent has been transferred onto the fibers. The fastness properties in terms of washing and light of the used bamboo fibers are rated as average (3-4) to good (4). It is a clear indication that these used fibers can be further used for manufacturing various utility products, that is, foot mats/rugs, composite sheets, colored papers, decorative book binding clothes, and wrapping paper, and can be blended with other bast fibers. This will further reduce the load on the environment in terms of dumping of used adsorbents after their use like another synthetic adsorbent.

3.12. Comparing This Adsorbent to Others. Very scanty work has been reported on the removal of Reactive Blue 235 dye using the adsorption process. Although Reactive Blue 235 is a widely used dye in the textile industry, adsorption is the most cost-effective, simple, easy and widely used technique for the removal of dye. From literature survey [117], it is observed that only one adsorbent has been used for removing Reactive Blue 235 dye. In this reported study, the optimum time required for the removal process is 240 minutes which is higher than the optimum contact time (40 minutes) used in present study.

When compared to the other adsorbent material, Table 13 indicates that BAT is a worthy adsorbent that can be used for the removal of Reactive Blue 235 from wastewater.

4. Conclusions

In this pioneering study, we delved into the transformative potential of cetyltrimethylammonium bromide (CTAB) modified bamboo fibers, sourced from local waste streams, as a highly effective adsorbent for eliminating Reactive Blue 235 from textile effluent. The central focus on utilizing bamboo, a readily available and renewable local resource, serves as the cornerstone of our commitment to sustainability.

Our exhaustive characterization of the adsorbent (BAT) through techniques such as FT-IR, Powder-XRD, SEM, Brunauer–Emmett–Teller (BET) analysis, and thermogravimetric analysis provided a detailed understanding of its structural and chemical properties. Notably, the percentage of dye removal demonstrated a direct correlation with both the initial dye concentration and the dosage of the adsorbent.

BAT's exceptional efficiency was underscored by its ability to remove over 80% of the dye within a remarkably short contact time of just 10 minutes. The influence of pH emerged as a critical factor, with optimal results achieved at lower pH values.

Adsorbent dosage of 0.5 g/50 ml of dye solution, initial dye concentration of 40 mg/L, pH of 6, and contact time of 40 minutes were found to yield the best dye removal efficiency of 94% for Reactive Blue 235.

The pseudo-second-order and Langmuir adsorption models effectively described the adsorption mechanism, affirming the favorable nature of Reactive Blue 235 adsorption on BAT.

Our nuanced exploration of the boundary layer effect, as evidenced by the graph of q_t versus $t^{1/2}$ not passing through the origin, provided insights into the multifaceted nature of the rate-limiting steps. The Temkin isotherm and Dubinin–Radushkevich (DR) isotherm models revealed temperature-dependent variations, highlighting the physicochemical essence of the adsorption process.

The thermodynamic analysis offered additional depth, unveiling the spontaneity of the adsorption process driven by positive entropy (ΔS). The obtained values of ΔH and ΔG indicated a physicochemical adsorption process, affirming the versatility and adaptability of BAT.

In conclusion, our study advocates for the adoption of CTAB-modified bamboo fibers, derived from locally available waste bamboo, as a compelling and eco-friendly solution for textile effluent treatment. Beyond addressing effluent pollution, this approach champions the repurposing of local waste materials, aligning with the principles of sustainability and environmental stewardship. Through the utilization of indigenous resources, our research contributes to the paradigm shift towards more sustainable practices in the realm of environmental remediation.

Data Availability

Data will be made available in case of request.

Conflicts of Interest

The authors declare that they have no conflicts of interest.

Acknowledgments

We are grateful to the DST-SERB Power Grant (DST No: SPG/2021/000857) and DST for Woman Scientist Fellowship (File No. DST/WOS-A/CS-64/2021) for providing the financial support.

References

- [1] D. R. Lima, L. Klein, and G. L. Dotto, "Application of ultrasound modified corn straw as adsorbent for malachite green removal from synthetic and real effluents," *Environmental Science and Pollution Research*, vol. 24, no. 26, pp. 21484–21495, 2017.
- [2] A. K. Verma, R. R. Dash, and P. Bhunia, "A review on chemical coagulation/flocculation technologies for removal

- of Colour from textile wastewaters," *Journal of Environmental Management*, vol. 93, no. 1, pp. 154–168, 2012.
- [3] S. Selambakkannu, N. A. F. Othman, K. A. Bakar, and Z. A. Karim, "Adsorption studies of packed bed column for the removal of dyes using amine functionalized radiation induced grafted fiber," *SN Applied Sciences*, vol. 1, no. 2, p. 175, 2019.
- [4] M. M. Hassan and C. M. Carr, "A critical review on recent advancements of the removal of reactive dyes from dye house effluent by ion-exchange adsorbents," *Chemosphere*, vol. 209, pp. 201–219, 2018.
- [5] S. Benkhaya, S. M'rabet, and A. El Harfi, "A review on classifications, recent synthesis and applications of textile dyes," *Inorganic Chemistry Communications*, vol. 115, Article ID 107891, 2020.
- [6] V. V. Chandanshive, S. K. Kadam, R. V. Khandare et al., "In situ phytoremediation of dyes from textile wastewater using garden ornamental plants, effect on soil quality and plant growth," *Chemosphere*, vol. 210, pp. 968–976, 2018.
- [7] A. Guediri, A. Bouguettoucha, D. Chebli, N. Chafai, and A. Amrane, "Molecular dynamic simulation and DFT computational studies on the adsorption performances of methylene blue in aqueous solutions by orange peel-modified phosphoric acid," *Journal of Molecular Structure*, vol. 1202, Article ID 127290, 2020.
- [8] D. Balarak, T. J. Al-Musawi, I. A. Mohammed, and H. Abasizadeh, "The eradication of reactive black 5 dye liquid wastes using *Azolla filiculoides* aquatic fern as a good and an economical biosorption agent," *SN Applied Sciences*, vol. 2, no. 6, p. 1015, 2020.
- [9] Y. S. Al-Degs, M. Elbarghouthi, A. H. El-Sheikh, and G. M. Walker, "Effect of solution pH, ionic strength, and temperature on adsorption behavior of reactive dyes on activated carbon," *Dyes and Pigments*, vol. 77, no. 1, pp. 16–23, 2008.
- [10] K. Santhy and P. Selvathy, "Removal of reactive dyes from wastewater by adsorption on coir pith activated carbon on coir pith activated carbon," *Bioresource Technology*, vol. 97, no. 11, pp. 1329–1336, 2006.
- [11] N. Nippatla and L. Philip, "Electrocoagulation-floatation assisted pulsed power plasma technology for the complete mineralization of potentially toxic dyes and real textile wastewater," *Process Safety and Environmental Protection*, vol. 125, pp. 143–156, 2019.
- [12] D. Balarak, F. Ganji, S. S. Choi, S. M. Lee, and M. J. Shim, "Effects of operational parameters on the removal of acid blue 25 dye from aqueous solutions by electrocoagulation," *Applied Chemistry for Engineering*, vol. 30, no. 6, pp. 742–748, 2019.
- [13] Y. Li, Y. Zhou, Y. Zhou, J. Lei, and S. Pu, "Cyclodextrin modified filter paper for removal of cationic dyes/Cu ions from aqueous solutions," *Water Science and Technology*, vol. 78, no. 12, pp. 2553–2563, 2018.
- [14] S. H. Tang and M. A. A. Zaini, "Microporous activated carbon prepared from yarn processing sludge via composite chemical activation for excellent adsorptive removal of malachite green," *Surfaces and Interfaces*, vol. 22, Article ID 100832, 2021.
- [15] T. G. Bulc and A. Ojstrsek, "The use of constructed wetland for dye-rich textile wastewater treatment," *Journal of Hazardous Materials*, vol. 155, no. 1-2, pp. 76–82, 2008.
- [16] H. C. Tee, P. E. Lim, C. E. Seng, M. A. Mohd Nawi, and R. Adnan, "Enhancement of azo dye Acid Orange 7 removal in newly developed horizontal subsurface-flow constructed wetland," *Journal of Environmental Management*, vol. 147, pp. 349–355, 2015.
- [17] N. Firdous, I. A. Shaikh, and R. Shahid, "Decolorization of reactive azo dye Remazol black B by using advanced oxidation processes (AOPs)," *Journal of the Chemical Society of Pakistan*, vol. 40, no. 05, pp. 828–833, 2018.
- [18] T. J. Al-Musawi, P. Rajiv, N. Mengelizadeh, I. A. Mohammed, and D. Balarak, "Development of sonophotocatalytic process for degradation of acid orange 7 dye by using titanium dioxide nanoparticles/graphene oxide nanocomposite as a catalyst," *Journal of Environmental Management*, vol. 292, Article ID 112777, 2021.
- [19] H. C. Chu and K. M. Chen, "Reuse of activated sludge biomass: I. Removal of basic dyes from wastewater by biomass," *Process Biochemistry*, vol. 37, no. 6, pp. 595–600, 2002.
- [20] K. Meerbergen, S. Crauwels, K. A. Willems et al., "Decolorization of reactive azo dyes using a sequential chemical and activated sludge treatment," *Journal of Bioscience and Bioengineering*, vol. 124, no. 6, pp. 668–673, 2017.
- [21] S. Sirianuntapiboon, K. Chairattawan, and S. Jungphongsukpanich, "Some properties of a sequencing batch reactor system for removal of vat dyes," *Bioresource Technology*, vol. 97, no. 10, pp. 1243–1252, 2006.
- [22] B. Chamam, M. Heran, R. B. Amar, and A. Grasmick, "Comparison of textile dye treatment by biosorption and membrane bioreactor," *Environmental Technology*, vol. 28, no. 12, pp. 1325–1331, 2007.
- [23] S. Karcher, A. Kornmuller, and M. Jekel, "Anion exchange resins for removal of reactive dyes from textile wastewaters," *Water Research*, vol. 36, no. 19, pp. 4717–4724, 2002.
- [24] N. M. Marin, O. Tiron, L. F. Pascu, M. Costache, M. Nita Lazar, and I. A. Badea, "Synergistic methodology based on ion exchange and biodegradation mechanisms applied for metal complex dye removal from waste waters," *Revista de Chimie*, vol. 69, no. 1, pp. 38–44, 2018.
- [25] A. Noor, A. Khan, H. N. Bhatti et al., "Polypyrrole and rice husk composite potential for the adsorptive removal of 2,4,6-trichloro phenol from aqueous medium," *Arabian Journal of Chemistry*, vol. 15, no. 12, Article ID 104352, 2022.
- [26] S. Dutta, B. Gupta, S. K. Srivastava, and A. K. Gupta, "Recent advances on the removal of dyes from wastewater using various adsorbents: a critical review," *Materials Advances*, vol. 2, no. 14, pp. 4497–4531, 2021.
- [27] D. Sun, Z. Zhang, M. Wang, and Y. Wu, "Adsorption of reactive dyes on activated carbon developed from & enteromorpha prolifera," *American Journal of Analytical Chemistry*, vol. 04, no. 07, pp. 17–26, 2013.
- [28] S. S. Lam, R. K. Liew, Y. M. Wong et al., "Microwave-assisted pyrolysis with chemical activation, an innovative method to convert orange peel into activated carbon with improved properties as dye adsorbent," *Journal of Cleaner Production*, vol. 162, pp. 1376–1387, 2017.
- [29] L. Ding, B. Zou, W. Gao et al., "Adsorption of Rhodamine-B from aqueous solution using treated rice husk-based activated carbon," *Colloids and Surfaces A: Physicochemical and Engineering Aspects*, vol. 446, pp. 1–7, 2014.
- [30] K. Song, H. Xu, L. Xu, K. Xie, and Y. Yang, "Cellulose nanocrystal-reinforced keratin bioadsorbent for effective removal of dyes from aqueous solution," *Bioresource Technology*, vol. 232, pp. 254–262, 2017.
- [31] V. Janaki, K. Vijayaraghavan, B. T. Oh et al., "Starch/polyaniline nanocomposite for enhanced removal of reactive

- dyes from synthetic effluent,” *Carbohydrate Polymers*, vol. 90, no. 4, pp. 1437–1444, 2012.
- [32] E. C. Lima, B. Royer, J. C. P. Vagheti et al., “Application of Brazilian pine-fruit shell as a biosorbent to removal of reactive red 194 textile dye from aqueous solution: kinetics and equilibrium study,” *Journal of Hazardous Materials*, vol. 155, no. 3, pp. 536–550, 2008.
- [33] S. M. de Oliveira Brito, H. M. C. Andrade, L. F. Soares, and R. P. de Azevedo, “Brazil nut shells as a new biosorbent to remove methylene blue and indigo carmine from aqueous solutions,” *Journal of Hazardous Materials*, vol. 174, no. 1-3, pp. 84–92, 2010.
- [34] S. T. Akar, A. S. Ozcan, T. Akar, A. Ozcan, and Z. Kaynak, “Biosorption of a reactive textile dye from aqueous solutions utilizing an agro-waste,” *Desalination*, vol. 249, no. 2, pp. 757–761, 2009.
- [35] D. Balarak, H. Abasizadeh, J. K. Yan, M. J. Shim, and S. M. Lee, “Biosorption of Acid Orange 7 (AO7) dye by canola waste: equilibrium, kinetic and thermodynamics studies,” *Treatment Desalination and Water*, vol. 190, pp. 331–339, 2020.
- [36] J. Abdi, M. Vossoughi, N. M. Mahmoodi, and I. Alemzadeh, “Synthesis of metal-organic framework hybrid nanocomposites based on GO and CNT with high adsorption capacity for dye removal,” *Chemical Engineering Journal*, vol. 326, pp. 1145–1158, 2017.
- [37] D. Balarak, M. Zafariyan, C. A. Igwegbe, K. K. Onyechi, and J. O. Ighalo, “Adsorption of acid blue 92 dye from aqueous solutions by single-walled carbon nanotubes: isothermal, kinetic, and thermodynamic studies,” *Environmental Processes*, vol. 8, no. 2, pp. 869–888, 2021.
- [38] A. N. Chowdhury, S. R. Jesmeen, and M. M. Hossain, “Removal of dyes from water by conducting polymeric adsorbent,” *Polymers for Advanced Technologies*, vol. 15, no. 11, pp. 633–638, 2004.
- [39] K. T. Kubra, M. S. Salman, and M. N. Hasan, “Enhanced toxic dye removal from wastewater using biodegradable polymeric natural adsorbent,” *Journal of Molecular Liquids*, vol. 328, Article ID 115468, 2021.
- [40] A. W. M. Ip, J. P. Barford, and G. McKay, “Reactive Black dye adsorption/desorption onto different adsorbents: effect of salt, surface chemistry, pore size and surface area,” *Journal of Colloid and Interface Science*, vol. 337, no. 1, pp. 32–38, 2009.
- [41] C. Jarusiripot, “Removal of reactive dye by adsorption over chemical pretreatment coal based bottom ash,” *Procedia Chemistry*, vol. 9, pp. 121–130, 2014.
- [42] K. M. Mousa and A. H. Taha, “Adsorption of reactive blue dye onto natural and modified wheat straw,” *Journal of Chemical Engineering & Process Technology*, vol. 6, no. 6, 2016.
- [43] Q. Li, Q. Y. Yue, Y. Su, B. Y. Gao, and L. Fu, “Cationic polyelectrolyte/bentonite prepared by ultrasonic technique and its use as adsorbent for Reactive Blue K-GL dye,” *Journal of Hazardous Materials*, vol. 147, no. 1-2, pp. 370–380, 2007.
- [44] E. Natarajan and G. P. Ponnaiah, “Synthesis of iron oxide micro and nanoparticles from aluminum industry waste and its application in the decolorization of reactive blue 235 dye,” *Current Pharmaceutical Biotechnology*, vol. 17, no. 10, pp. 873–885, 2016.
- [45] G. M. Ratnamala, U. B. Deshannavar, S. Munyal, K. Tashildar, S. Patil, and A. Shinde, “Adsorption of reactive blue dye from aqueous solutions using sawdust as adsorbent: optimization, kinetic, and equilibrium studies,” *Arabian Journal for Science and Engineering*, vol. 41, no. 2, pp. 333–344, 2016.
- [46] S. C. R. Santos, V. J. P. Vilar, and R. A. R. Boaventura, “Waste metal hydroxide sludge as adsorbent for a reactive dye,” *Journal of Hazardous Materials*, vol. 153, no. 3, pp. 999–1008, 2008.
- [47] T. L. Silva, A. Ronix, O. Pezoti et al., “Mesoporous activated carbon from industrial laundry sewage sludge: adsorption studies of reactive dye Remazol Brilliant Blue R,” *Chemical Engineering Journal*, vol. 303, pp. 467–476, 2016.
- [48] M. H. Dehghani, A. Dehghan, and A. Najafpoor, “Removing Reactive Red 120 and 196 using chitosan/zeolite composite from aqueous solutions: kinetics, isotherms, and process optimization,” *Journal of Industrial and Engineering Chemistry*, vol. 51, pp. 185–195, 2017.
- [49] N. M. Mahmoodi, J. Abdi, and D. Bastani, “Direct dyes removal using modified magnetic ferrite nanoparticle,” *Journal of Environmental Health Science and Engineering*, vol. 12, pp. 96–10, 2014.
- [50] A. M. Youssef Am, A. M. Youssef, and M. M. Al-Awadhi, “Adsorption of acid dyes onto bentonite and surfactant-modified bentonite,” *Journal of Analytical & Bioanalytical Techniques*, vol. 04, no. 04, pp. 1–7, 2013.
- [51] M. Munir, M. F. Nazar, and M. N. Zafar, “Removal of amaranth dye over surfactant modified dull pink clay from aqueous medium,” *International Journal of Environmental Analytical Chemistry*, vol. 101, no. 15, pp. 2848–2865, 2021.
- [52] M. Jeeva and W. Y. Wan Zuhairi, “Adsorption of acid orange 33 dye by bentonite and surfactant modified bentonite,” *Asian Journal of Chemistry*, vol. 30, no. 11, pp. 2383–2388, 2018.
- [53] S. Sumanjit, R. K. Mahajan, R. Mahajan, and V. K. Gupta, “Modification of surface behaviour of *Eichhornia crassipes* using surface active agent: an adsorption study,” *Journal of Industrial and Engineering Chemistry*, vol. 21, pp. 189–197, 2015.
- [54] A. Alhujaily, H. Yu, X. Zhang, and F. Ma, “Highly efficient and sustainable spent mushroom waste adsorbent based on surfactant modification for the removal of toxic dyes,” *International Journal of Environmental Research and Public Health*, vol. 15, no. 7, p. 1421, 2018.
- [55] D. W. Astuti, N. H. Aprilita, and M. Mudasir, “Adsorption of the anionic dye of Congo red from aqueous solution using A modified natural zeolite with benzalkonium chloride,” *Rasayan Journal of Chemistry*, vol. 13, no. 02, pp. 845–853, 2020.
- [56] C. Namasivayam and M. V. Sureshkumar, “Anionic dye adsorption characteristics of surfactant-modified coir pith, a ‘waste’ lignocellulosic polymer,” *Journal of Applied Polymer Science*, vol. 100, no. 2, pp. 1538–1546, 2006.
- [57] M. Yazdani, N. M. Mahmoodi, M. Arami, and H. Bahrami, “Surfactant-modified feldspar: isotherm, kinetic, and thermodynamic of binary system dye removal,” *Journal of Applied Polymer Science*, vol. 126, no. 1, pp. 340–349, 2012.
- [58] R. Ansari, B. Seyghali, A. Mohammad-khah, and M. A. Zanjanchi, “Application of nano surfactant modified biosorbent as an efficient adsorbent for dye removal,” *Separation Science and Technology*, vol. 47, no. 12, pp. 1802–1812, 2012.
- [59] B. Zhang, Z. Dong, D. Sun, T. Wu, and Y. Li, “Enhanced adsorption capacity of dyes by surfactant-modified layered double hydroxides from aqueous solution,” *Journal of Industrial and Engineering Chemistry*, vol. 49, pp. 208–218, 2017.

- [60] M. R. Malekbala, M. A. Khan, S. Hosseini, L. C. Abdullah, and T. S. Y. Choong, "Adsorption/desorption of cationic dye on surfactant modified mesoporous carbon coated monolith: equilibrium, kinetic and thermodynamic studies," *Journal of Industrial and Engineering Chemistry*, vol. 21, pp. 369–377, 2015.
- [61] A. Asfaram, M. R. Fathi, S. Khodadoust, and M. Naraki, "Removal of Direct Red 12B by garlic peel as a cheap adsorbent: kinetics, thermodynamic and equilibrium isotherms study of removal," *Spectrochimica Acta Part A: Molecular and Biomolecular Spectroscopy*, vol. 127, pp. 415–421, 2014.
- [62] R. Sivaraj, C. Namasivayam, and K. Kadirvelu, "Orange peel as an adsorbent in the removal of acid violet 17 (acid dye) from aqueous solutions," *Waste Management*, vol. 21, no. 1, pp. 105–110, 2001.
- [63] K. Saed, M. J. M. M. Noor, and B. Yusuf, "Sugarcane bagasse as an adsorbent for dye material," *Journal of Industrial Pollution Control*, vol. 21, no. 1, pp. 1–10, 2005.
- [64] B. Saba, M. Jabeen, A. Khalid, I. Aziz, and A. Christy, "Effectiveness of rice agricultural waste, microbes and wetland plants in the removal of reactive black-5 azo dye in microcosm constructed wetlands," *International Journal of Phytoremediation*, vol. 17, no. 11, pp. 1060–1067, 2015.
- [65] J. Xiong, C. Jiao, C. Li, D. Zhang, H. Lin, and Y. Chen, "A versatile amphiprotic cotton fiber for the removal of dyes and metal ions," *Cellulose*, vol. 21, no. 4, pp. 3073–3087, 2014.
- [66] P. S. Syed Shabldeen, R. Venkatesh, S. Madhavakrishnan, K. K. Adirvelu, and S. Pattabhi, "Kapok hull as an adsorbent for acid dye removal," *Asian Journal of Microbiology, Biotechnology and Environmental Sciences*, vol. 9, no. 3, pp. 731–740, 2007.
- [67] S. Ethaib, I. K. Erabee, and A. A. Abdulsahib, "Removal of methylene blue dye from synthetic wastewater using kenaf core and activated carbon," *International Journal of Engineering & Technology*, vol. 7, no. 4.19, pp. 909–913, 2018.
- [68] A. Jumariah, T. Chuah, J. Gimbon, T. Choong, and I. Azni, "Adsorption of basic dye onto palm kernel shell activated carbon: sorption equilibrium and kinetics studies," *Desalination*, vol. 186, no. 1-3, pp. 57–64, 2005.
- [69] H. P. S. Abdul Khalil, I. U. H. Bhat, M. Jawaid, A. Zaidon, D. Hermawan, and Y. S. Hadi, "Bamboo fibre reinforced biocomposites: a review," *Materials & Design*, vol. 42, pp. 353–368, 2012.
- [70] Y. Jiao, C. Wan, and J. Li, "Synthesis of carbon fiber aerogel from natural bamboo fiber and its application as a green high-efficiency and recyclable adsorbent," *Materials & Design*, vol. 107, pp. 26–32, 2016.
- [71] W. Yuan, X. Zhang, J. Zhao et al., "Ultra-lightweight and highly porous carbon aerogels from bamboo pulp fibers as an effective sorbent for water treatment," *Results in Physics*, vol. 7, pp. 2919–2924, 2017.
- [72] S. Yang, L. Chen, L. Mu, B. Hao, and P. C. Ma, "Low cost carbon fiber aerogel derived from bamboo for the adsorption of oils and organic solvents with excellent performances," *RSC Advances*, vol. 5, no. 48, pp. 38470–38478, 2015.
- [73] H. Wang, Y. Gong, and Y. Wang, "Cellulose-based hydrophobic carbon aerogels as versatile and superior adsorbents for sewage treatment," *RSC Advances*, vol. 4, no. 86, pp. 45753–45759, 2014.
- [74] B. H. Hameed, A. T. M. Din, and A. L. Ahmad, "Adsorption of methylene blue onto bamboo-based activated carbon: kinetics and equilibrium studies," *Journal of Hazardous Materials*, vol. 141, no. 3, pp. 819–825, 2007.
- [75] X. Ma, L. M. Smith, L. Cai, S. Q. Shi, H. Li, and B. Fei, "Preparation of high-performance activated carbons using bamboo through one-step pyrolysis," *Bioresources*, vol. 14, no. 1, pp. 688–699, 2018.
- [76] L. S. Chan, W. H. Cheung, and G. McKay, "Adsorption of acid dyes by bamboo derived activated carbon," *Desalination*, vol. 218, no. 1-3, pp. 304–312, 2008.
- [77] F. Wu, R. Tseng, and R. Juang, "Preparation of activated carbons from bamboo and their adsorption abilities for dyes and phenol," *Journal of Environmental Science and Health, Part A*, vol. 34, no. 9, pp. 1753–1775, 1999.
- [78] J. Zhang, W. Lu, H. Li et al., "Polyethyleneimine-impregnated alkali treated waste bamboo powder for effective dye removal," *Water Science and Technology*, vol. 83, no. 5, pp. 1183–1197, 2021.
- [79] Y. Yang, X. Lin, B. Wei, Y. Zhao, and J. Wang, "Evaluation of adsorption potential of bamboo biochar for metal-complex dye: equilibrium, kinetics and artificial neural network modeling," *International journal of Environmental Science and Technology*, vol. 11, no. 4, pp. 1093–1100, 2014.
- [80] S. K. Ghosh and A. Bandyopadhyay, "Adsorption of methylene blue onto citric acid treated carbonized bamboo leaves powder: equilibrium, kinetics, thermodynamics analyses," *Journal of Molecular Liquids*, vol. 248, pp. 413–424, 2017.
- [81] J. Rivera-Utrilla, I. Bautista-Toledo, M. A. Ferro-García, and C. Moreno-Castilla, "Activated carbon surface modifications by adsorption of bacteria and their effect on aqueous lead adsorption," *Journal of Chemical Technology and Biotechnology*, vol. 76, no. 12, pp. 1209–1215, 2001.
- [82] H. P. Boehm, "Some aspects of the surface chemistry of carbon blacks and other carbons," *Carbon*, vol. 32, no. 5, pp. 759–769, 1994.
- [83] P. Tengvall, "Protein interactions with biomaterials," in *Comprehensive Biomaterials II*, P. Ducheyne, Ed., pp. 63–73, Elsevier, Amsterdam, Netherlands, 2011.
- [84] M. Nasiruddin Khan and A. Sarwar, "Determination of points of zero charge of natural and treated adsorbents," *Surface Review and Letters*, vol. 14, no. 03, pp. 461–469, 2007.
- [85] S. Bhattacharya, N. Bar, B. Rajbansi, and S. K. Das, "Synthesis of chitosan-nTiO₂ nanocomposite, application in adsorptive removal of Cu (II)—adsorption and desorption study, mechanism, scale-up design, statistical, and genetic algorithm modeling," *Applied Organometallic Chemistry*, vol. 37, no. 6, Article ID e7094, 2023.
- [86] M. I. Maulana, M. Marwanto, D. S. Nawawi, S. Nikmatin, F. Febrianto, and N. H. Kim, "Chemical components content of seven Indonesian bamboo Species," *IOP Conference Series: Materials Science and Engineering*, vol. 935, no. 1, Article ID 012028, 2020.
- [87] P. Gans, *Vibrating Molecules: An Introduction to the Interpretation of Infrared and Raman Spectra*, Chapman & Hall, London, UK, 1975.
- [88] J. R. Njimou, A. Măicăneanu, C. Indolean, C. P. Nansu-Njiki, and E. Ngameni, "Removal of Cd (II) from synthetic wastewater by alginate-Ayous wood sawdust (Triplachiton scleroxylon) composite material," *Environmental Technology*, vol. 37, no. 11, pp. 1369–1381, 2016.
- [89] B. D. Cullity, *Elements of X-Ray Diffraction*, Addison-Wesley Publishing Company, Massachusetts, MA, USA, 1956.

- [90] S. J. Salih, A. S. Abdul Kareem, and S. S. Anwer, "Adsorption of anionic dyes from textile wastewater utilizing raw corn-cob," *Heliyon*, vol. 8, no. 8, Article ID 10092, 2022.
- [91] J. Godwin, J. R. Njimou, N. Abdus-Salam et al., "Nanoscale ZnO-adsorbent carefully designed for the kinetic and thermodynamic studies of Rhodamine B," *Inorganic Chemistry Communications*, vol. 138, Article ID 109287, 2022.
- [92] S. Netpradit, P. Thiravetyan, and S. Towprayoon, "Adsorption of three azo reactive dyes by metal hydroxide sludge: effect of temperature, pH, and electrolytes," *Journal of Colloid and Interface Science*, vol. 270, no. 2, pp. 255–261, 2004.
- [93] D. Karadag, E. Akgul, S. Tok, F. Erturk, M. A. Kaya, and M. Turan, "Basic and reactive dye removal using natural and modified zeolites," *Journal of Chemical & Engineering Data*, vol. 52, no. 6, pp. 2436–2441, 2007.
- [94] W. J. Weber and J. C. Morris, "Kinetics of adsorption on carbon from solution," *Journal of the Sanitary Engineering Division*, vol. 89, no. 2, pp. 31–59, 1963.
- [95] G. E. Boyd, A. W. Adamson, and L. S. Myers, "The exchange adsorption of ions from aqueous solutions by organic zeolites. II. Kinetics," *Journal of the American Chemical Society*, vol. 69, no. 11, pp. 2836–2848, 1947.
- [96] A. Mittal, J. Mittal, A. Malviya, and V. K. Gupta, "Adsorptive removal of hazardous anionic dye Congo red from wastewater using waste materials and recovery by desorption," *Journal of Colloid and Interface Science*, vol. 340, no. 1, pp. 16–26, 2009.
- [97] X. S. Wang, Z. Z. Li, and S. R. Tao, "Removal of chromium (VI) from aqueous solution using walnut hull," *Journal of Environmental Management*, vol. 90, no. 2, pp. 721–729, 2009.
- [98] S. R. Sumanjit, S. Rani, and R. Mahajan, "Equilibrium, kinetics and thermodynamic parameters for adsorptive removal of dye Basic Blue 9 by ground nut shells and Eichhornia," *Arabian Journal of Chemistry*, vol. 9, pp. 1464–1477, 2016.
- [99] A. Dąbrowski, "Adsorption-from theory to practice," *Advances in Colloid and Interface Science*, vol. 93, no. 1-3, pp. 135–224, 2001.
- [100] J. R. Njimou, J. Godwin, H. Pahimi et al., "Biocomposite spheres based on aluminum oxide dispersed with orange-peel powder for adsorption of phenol from batch membrane fraction of olive mill wastewater," *Colloid and Interface Science Communications*, vol. 42, Article ID 100402, 2021.
- [101] H. K. Boparai, M. Joseph, and D. M. O'Carroll, "Kinetics and thermodynamics of cadmium ion removal by adsorption onto nano zerovalent iron particles," *Journal of Hazardous Materials*, vol. 186, no. 1, pp. 458–465, 2011.
- [102] G. Crini, "Kinetic and equilibrium studies on the removal of cationic dyes from aqueous solution by adsorption onto a cyclodextrin polymer," *Dyes and Pigments*, vol. 77, no. 2, pp. 415–426, 2008.
- [103] R. D. Johnson and F. H. Arnold, "The Temkin isotherm describes heterogeneous protein adsorption," *Biochimica et Biophysica Acta (BBA) Protein Structure and Molecular Enzymology*, vol. 1247, no. 2, pp. 293–297, 1995.
- [104] A. A. Inyinbor, F. A. Adekola, and G. A. Olatunji, "Kinetics, isotherms and thermodynamic modeling of liquid phase adsorption of Rhodamine B dye onto Raphia hookerie fruit epicarp," *Water Resources and Industry*, vol. 15, pp. 14–27, 2016.
- [105] S. Kaur, S. Rani, and R. K. Mahajan, "Adsorptive removal of dye crystal violet onto low-cost carbon produced from Eichhornia plant: kinetic, equilibrium, and thermodynamic studies," *Desalination and Water Treatment*, vol. 53, no. 2, pp. 543–556, 2015.
- [106] J. R. Njimou, M. Pengou, H. K. Tchakoute et al., "Removal of lead ions from aqueous solution using phosphate-based geopolymer cement composite," *Journal of Chemical Technology and Biotechnology*, vol. 96, no. 5, pp. 1358–1369, 2021.
- [107] N. Ayawei, A. T. Ekubo, D. Wankasi, and E. D. Dikio, "Adsorption of Congo red by Ni/Al-CO₃: equilibrium, thermodynamic and kinetic studies," *Oriental Journal of Chemistry*, vol. 31, no. 3, pp. 1307–1318, 2015.
- [108] A. Altinisik, E. Gur, and Y. Seki, "A natural sorbent, *Luffa cylindrica* for the removal of a model basic dye," *Journal of Hazardous Materials*, vol. 179, no. 1-3, pp. 658–664, 2010.
- [109] Q. Huang, D. Hu, M. Chen, C. Bao, and X. Jin, "Sequential removal of aniline and heavy metal ions by jute fiber biosorbents: a practical design of modifying adsorbent with reactive adsorbate," *Journal of Molecular Liquids*, vol. 285, pp. 288–298, 2019.
- [110] S. Rajoriya, V. K. Saharan, A. S. Pundir, M. Nigam, and K. Roy, "Adsorption of methyl red dye from aqueous solution onto eggshell waste material: kinetics, isotherms and thermodynamic studies," *Current Research in Green and Sustainable Chemistry*, vol. 4, Article ID 100180, 2021.
- [111] R. S. Mane and V. N. Bhusari, "Removal of Colour (dyes) from textile effluent by adsorption using Orange and Banana peel," *International Journal of Engineering Research in Africa*, vol. 2, no. 3, pp. 1997–2004, 2012.
- [112] N. Ayawei, A. N. Ebelegi, and D. Wankasi, "Modelling and interpretation of adsorption isotherms," *Journal of Chemistry*, vol. 2017, Article ID 3039817, 11 pages, 2017.
- [113] A. K. Dey, A. Dey, and R. Goswami, "Selection of optimal performance characteristics during adsorption of Methyl red dye using sodium carbonate treated jute fibre," *Desalination and Water Treatment*, vol. 260, pp. 187–202, 2022.
- [114] S. De Gisi, G. Lofrano, M. Grassi, and M. Notarnicola, "Characteristics and adsorption capacities of low-cost sorbents for wastewater treatment: a review," *Sustainable Materials and Technologies*, vol. 9, pp. 10–40, 2016.
- [115] V. A. Shenai and M. Saraf, *Principles & Practice of DYEING*, Sevak publications, Mumbai, India, 1991.
- [116] A. Das, N. Bar, and S. K. Das, "Adsorptive removal of Pb(II) ion on *Arachis hypogaea*'s shell: batch Experiments, statistical, and GA modeling," *International journal of Environmental Science and Technology*, vol. 20, no. 1, pp. 537–550, 2023.
- [117] E. Natarajan and G. P. Ponnaiah, "Optimization of process parameters for the decolorization of Reactive Blue 235 dye by barium alginate immobilized iron nanoparticles synthesized from aluminum industry waste," *Environmental Nanotechnology, Monitoring & Management*, vol. 7, pp. 73–88, 2017.